https://doi.org/10.5194/egusphere-2026-6903
Preprint. Discussion started: 12 November 2026
© Author(s) 2026. CC BY 4.0 License.

Characterising week-long South American biomass burning plume transport and in-plume formic acid evolution using IASI measurements and chemical box model

Maria P. Velásquez-García[1,2], Richard J. Pope[1,2], Steven T. Turnock[3,4], Steve R. Arnold[1], David P. Moore[5,6], Ruth M. Doherty[7], Ailish M. Graham[1,2], John J. Remedios[5,6], and Martyn P. Chipperfield[1,2]

[1]School of Earth, Environment and Sustainability, University of Leeds, Leeds, UK
[2]National Centre for Earth Observation, University of Leeds, Leeds, UK
[3]Met Office Hadley Centre, Exeter, UK
[4]MetOffice@Leeds, School of Earth, Environment and Sustainability, University of Leeds, UK
[5]School of Physics and Astronomy, University of Leicester, Leicester, UK
[6]National Centre for Earth Observation, University of Leicester, Leicester, UK
[7]School of GeoSciences, University of Edinburgh, Edinburgh, UK

Correspondence: Maria P. Velásquez-García (eempvg@leeds.ac.uk)

Abstract. Formic acid (HCOOH) is a prevalent organic acid that influences rain acidity and aerosol properties. However, models largely underestimate its atmospheric abundance, particularly in biomass burning plumes. Here, we use the Infrared Atmospheric Sounding Interferometer (IASI) to track HCOOH evolution in ageing South American biomass burning plumes during the exceptionally active 2024 fire season. By integrating IASI retrievals of total column HCOOH (TCHCOOH) and carbon monoxide (TCCO) with atmospheric trajectory modelling, we analyse HCOOH changes over the rarely studied week-long period. We particularly focus on the free troposphere, consistent with satellite sensitivity and reported transport altitudes. We find that HCOOH formation is most pronounced between the day of emission (Day 0) and the following day (Day 1), with the TCHCOOH:TCCO ratio increasing by $\sim$5.7 $\pm$ 1.0% day^{-1}. Between Day 2 and Day 6, the TCHCOOH:TCCO ratio decays at $\sim$4.8 $\pm$ 0.8 % day^{-1} as HCOOH is lost, then stabilises by Day 8. Box modelling based on the UK Chemistry and Aerosol model, initialised in the free troposphere (850 hPa) using in-plume observations, captures the increase in HCOOH:CO on the first day (4.4% day^{-1}) but slightly underestimates it. The model identifies hydroxymethyl-methyl-α-lactone (HMML, an isoprene oxidation product), ethene, and acetylene as key HCOOH precursors. HMML might be influenced by vegetation-derived emissions. After Day 1, the simulated HCOOH:CO ratio declines smoothly (2.7% day^{-1}), dominated by OH oxidation. This work demonstrates a novel approach that combines different observations and methods to investigate atmospheric chemistry in biomass burning plumes over week-long timescales.

1 Introduction

Formic acid (HCOOH) is a ubiquitous volatile organic compound (VOC) in the troposphere. As an organic acid, it plays an important role in regulating atmospheric acidity, particularly in natural environments (Andreae et al., 1988). Over boreal forests, HCOOH reduces rainwater pH by 0.25 to 0.5 units (Stavrakou et al., 2012). As a result, HCOOH can limit pH-dependent

https://doi.org/10.5194/egusphere-2026-6903
Preprint. Discussion started: 12 November 2026
© Author(s) 2026. CC BY 4.0 License.

reactions in clouds and on aqueous aerosol surfaces (Jang et al., 2002; Surratt et al., 2007; Tilgner et al., 2021). Additionally, HCOOH influences the hygroscopic properties of aerosols (Silva et al., 2022; Tan et al., 2024), potentially contributing to cloud condensation nuclei abundance (Yu, 2000). The direct sources of HCOOH include fossil fuel combustion (Friedman et al., 2017), biomass burning (R'honi et al., 2013), and emissions from soil (Sanhueza and Andreae, 1991) and plants (Kesselmeier et al., 1998). The photochemical oxidation of biogenic (e.g. isoprene, ethene and monoterpenes) and non-biogenic (e.g. acetylene) VOCs contributes significantly to secondary HCOOH production (Millet et al., 2015; Stavrakou et al., 2012) and occurs via reaction with the hydroxyl radical (·OH) or ozonolysis, depending on the compound (Millet et al., 2015). HCOOH is largely lost by wet and dry deposition within the boundary layer, limiting the lifetime of HCOOH to 2-4 days (Franco et al., 2021). In the free troposphere, oxidation by the OH radical is the dominant sink (Millet et al., 2015; Paulot et al., 2011) and the HCOOH lifetime increases to ∼25 days (Franco et al., 2021). Based on known HCOOH sinks and sources, modelled HCOOH concentrations regularly underestimate ambient observations by a factor of three, pointing to an unknown production source (Franco et al., 2021; Millet et al., 2015; Stavrakou et al., 2012). Aqueous-phase oxidation and heterogeneous reactions on aerosols have been suggested as significant sources of HCOOH that might help to close the budget (Cope et al., 2021; Franco et al., 2021; Jiang et al., 2023), however, these sources remain uncertain and have been challenged (Nguyen et al., 2023).

Models particularly underestimate observed HCOOH abundances in biomass burning plumes, with simulations showing HCOOH magnitudes to be underestimated by a factor of 4-10 in these plumes (Chaliyakunnel et al., 2016; Permar et al., 2023), especially in the tropics. This discrepancy has been attributed to the secondary formation of HCOOH (R'honi et al., 2013; Wizenberg et al., 2023; Yamanouchi et al., 2020), and an overall underestimation of the amount of HCOOH emitted from fires (Viatte et al., 2015; Wizenberg et al., 2023). Investigations have revealed that the concentrations of HCOOH in biomass burning plumes can be two orders of magnitude higher than expected from emissions alone (Chen et al., 2021). In the extratropics, modelling by Wizenberg et al. (2023) captured observed HCOOH magnitudes in biomass-burning plumes but struggled to capture their variability.

Studies of HCOOH in biomass-burning plumes have frequently relied on observations from aircraft campaigns (e.g., Chen et al., 2021; Johansson et al., 2022) and ground-based Fourier transform infrared (FTIR) spectrometers (e.g., Viatte et al., 2015; Yamanouchi et al., 2020). Supported by laboratory experiments, these approaches have provided important insights into the chemical processes controlling HCOOH production and loss (e.g., Zhang et al., 2025). Over the past two decades, satellite observations have enabled the retrieval of HCOOH total columns, substantially expanding the spatial coverage of observations and providing valuable constraints for atmospheric models and biomass-burning emission estimates through the derivation of emission factors (e.g., Pommier et al., 2017; Tereszchuk et al., 2011). However, satellite observations have rarely been exploited to investigate the fate of HCOOH within biomass-burning plumes. This represents an important gap, as the detailed measurements provided by aircraft and FTIR instruments are generally limited to short observational periods and spatially restricted segments of a plume, typically spanning less than a day. Consequently, these approaches are often insufficient to track the evolution of HCOOH over the days-to-weeks timescales relevant to plume ageing and transport. However, satellite retrievals can provide a valuable complementary perspective, enabling the investigation of processes controlling HCOOH

https://doi.org/10.5194/egusphere-2026-6903
Preprint. Discussion started: 12 November 2026
© Author(s) 2026. CC BY 4.0 License.

evolution in biomass-burning plumes over regional scales and over the week-long timescales characteristic of its atmospheric variability (Chen et al., 2021).

This study aims to characterise and assess the evolution of HCOOH in biomass-burning plumes as they age and are transported during the week after emissions, using satellite retrievals from the Infrared Atmospheric Sounding Interferometer (IASI). Our analysis centres on South American plumes, since this region, together with Africa, experiences the highest annual abundance of biomass-burning-derived HCOOH in the southern tropics and midlatitudes (Glatthor et al., 2025). Specifically, we examine the August to October 2024 fire season, a period marked by long-range transport of large-scale biomass burning plumes that extended across the Atlantic (see example in Fig. 1). This period was preceded by record-breaking drought conditions over tropical South America (Signori et al., 2026; Barkhordarian et al., 2025), which triggered an exceptionally high number of fires in the region, including in key ecosystems such as the Amazon and Pantanal (Belém et al., 2026; Bourgoin et al., 2025). To provide a comprehensive understanding, we integrate data from meteorological reanalysis and retrievals of Aerosol Optical Depth (AOD) from the Moderate Resolution Imaging Spectroradiometer (MODIS), alongside IASI satellite retrievals of HCOOH and carbon monoxide (CO). We characterised biomass-burning plumes during the period using atmospheric trajectory modelling, and analysed HCOOH chemistry with the United Kingdom Chemistry and Aerosol (UKCA) box model.

2 Methods

This study investigates atmospheric HCOOH levels during the South American fire season (August to October) of 2024. During this time period, biomass burning plumes were frequently transported within South America and extended out over both the Pacific and Atlantic oceans, with some reaching Africa. As illustrated in Fig. 1, elevated total columns of HCOOH and CO, averaged over a 7-day period, reveal a large biomass burning plume moving from South America across the Atlantic. To quantify the spatial and temporal evolution of HCOOH levels, we analysed total column carbon monoxide (TCCO) and total column formic acid (TCHCOOH) data, along with AOD, as detailed in Sections 2.1 and 2.2. In addition, we used an atmospheric transport model to compute forward air mass trajectories to isolate and characterise the biomass burning plumes as described in Sections 2.3 and 2.4. We completed the study by conducting chemical box-model simulations of idealised plumes with representative conditions; the details are described in Section 2.5.

2.1 IASI-Retrieved Total Columns of HCOOH and CO

Satellite-retrieved measurements of TCHCOOH and TCCO were utilised to identify biomass burning plumes and quantify HCOOH variability within them. CO is a key tracer of biomass burning combustion and is commonly used to define the variation of more reactive tracers, as CO can persist in the atmosphere for 1-3 months after emission (Duncan et al., 2007). Consequently, for analysis on a one-week scale, CO is expected to be relatively stable. For this study, we used the TCHCOOH and TCCO retrieved by the University of Leicester IASI Retrieval Scheme (ULIRS) (Illingworth et al., 2011). ULIRS employs an optimal estimation approach to retrieve trace-gas profiles from IASI-measured radiances using radiances simulated by the

https://doi.org/10.5194/egusphere-2026-6903
Preprint. Discussion started: 12 November 2026
© Author(s) 2026. CC BY 4.0 License.

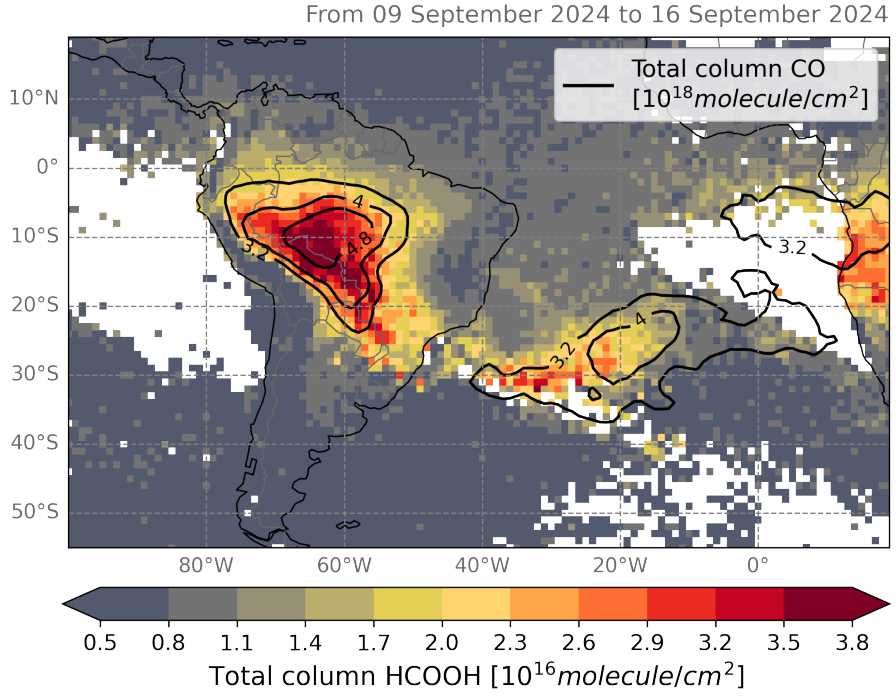


Figure 1. Median total column HCOOH [10^{16} molecules cm^{-2}] (background colours) and total column CO [10^{18} molecules cm^{-2}] (black contour lines) from 9^{th} September to 16^{th} September 2024 (illustrative plumes). White indicates that no data were available to calculate a median value at the pixel.

Reference Forward Model (Dudhia, 2017). To retrieve TCHCOOH, ULIRS uses seven different absorption bands: 1082-1090 cm^{-1}, 1092.5-1093.5 cm^{-1}, 1095.5-1098 cm^{-1}, 1103-1106 cm^{-1}, 1109-1109.75 cm^{-1}, 1113-1119 cm^{-1}1 and 1123-1134 cm^{-1}. For TCCO, ULIRS uses the broadband 2143-2181 cm^{-1}. The sensitivity of IASI near the surface is limited; on average, the vertical sensitivity of the product peaks at 250 hPa for TCHCOOH and 700 hPa and 200 hPa for TCCO (see Fig. S1). This sensitivity intrinsically defines biomass burning plumes closer to the mid-troposphere as the focus of this study.

TCHCOOH and TCCO are retrieved from the IASI sensors on board MetOp-B and MetOp-C. These two MetOp satellites are sun-synchronised, polar-orbiting satellites that cross the equator at their ascending and descending nodes at approximately 21:30 and 9:30 local time, respectively. For this study, the ULIRS retrievals were gridded onto a 1.0°×1.0° grid. The products provide a measure of the degree of freedom signal (DOFS) for the retrieved total columns, indicating the extent to which the retrieved columns are dominated by their a priori profile. Only retrievals with DOFS > 0.5 were used, ensuring that the retrieved product contained a meaningful independent signal from the satellite measurement rather than being dominated by the a priori information. For these products, ULIRS operational data quality filtering removed pixels with cloud cover greater than 25%.

This study presents the first scientific application of the ULIRS TCHCOOH product. To assess its performance, we compared the product with geographically and contextually relevant ground FTIR retrievals of TCHCOOH from the Belgian Institute for

https://doi.org/10.5194/egusphere-2026-6903
Preprint. Discussion started: 12 November 2026
© Author(s) 2026. CC BY 4.0 License.

Space Aeronomy (BIRA-IASB) in Porto Velho, Brazil (Vigouroux et al., 2021) during the 2019 fire season. This comparison shows good accuracy for the ULIRS product (see Fig. S2), yielding a Spearman correlation of 0.88 between the FTIR-retrieved TCHCOOH and the IASI-derived average TCHCOOH within 3 hours and 100 km of the FTIR measurement. However, ULIRS tended to underestimate TCHCOOH compared to the ground-based retrieval, with a mean bias of 27%. Further details of the comparison are provided in Text S1.

2.2 MODIS Aerosol Optical Depth

We used AOD to detect aerosols in the biomass burning plume, which may act as a potential precursor of HCOOH formation (Cope et al., 2021; Jiang et al., 2023; Zhang et al., 2025). We utilised the MODIS Aerosol Collection 6.1 products MOD04_L2 and MYD04_L2, obtained from Terra and Aqua, respectively (NASA, 2021). These are daily Level 2 datasets at 10 km resolution. Specifically, we adopted the AOD 550nm dark target deep blue combined product, which integrates differential quality filters for land and ocean to deliver a high-quality product. We resampled the product to the same 1.0°×1.0° grid used for TCHCOOH and TCCO, using nearest-neighbor method.

2.3 Fire activity and forward trajectories

We combine satellite data and atmospheric trajectory modelling to investigate the origin, atmospheric transport, and temporal evolution of biomass burning plumes. We used MODIS active fire hotspots to identify where fire events began across South America during our study period. We used only hotspots with a confidence level greater than 80%, as these indicate high confidence that the hotspot represents surface vegetation burning (Giglio, 2013). To account for fires that likely contribute to large magnitude emissions, we filtered hotspots by fire radiative power (FRP). Active fires with an FRP greater than the 75^{th} percentile of the data (100 MW) were selected. From this, we created a $1.0° \times 1.0°$ density map of fire occurrence for the three studied months. From the density map, we selected pixels with accumulated hotspots greater than 15. This aimed to identify large and/or frequent sources. We used the resulting 474 pixels as release locations to calculate air-mass forward trajectories.

For the release altitudes of the forward trajectories, we used the two plume injection height products from the Global Fire Assimilation System (GFAS) (CAMS, 2022). The first product is produced by the Monitoring and Modelling System for wildland fires (IS4FIRES), while the second is produced by a one-dimensional plume rise model as the "mean height of max injection" (Rémy et al., 2017). Both products are suitable for describing the plume injection height, and each has individual strengths that make them complementary for this analysis (Rémy et al., 2017). The product heights, in meters, were converted to pressure levels using surface temperature and pressure from meteorological reanalysis from the European Centre for Medium-Range Weather Forecasts 5th Generation Atmospheric Reanalysis (ERA5). For this, we used the barometric equation assuming that temperature decreases linearly with height at a lapse rate of 6.2 K km^{-1} (Mokhov and Akperov, 2006). From the products, we calculated the most frequent injection altitudes and used them as the release altitudes for each point extracted from the 3-month density map.

Once release points were defined, we ran forward trajectories using the Reading Offline Trajectory Code (ROTRAJ) (Methven et al., 2003), which computes air-mass trajectories from the ERA5 reanalysis. The forward trajectories were run for 240 hours

https://doi.org/10.5194/egusphere-2026-6903
Preprint. Discussion started: 12 November 2026
© Author(s) 2026. CC BY 4.0 License.

(i.e., 10 days) with a time step of 3 hours. A new forward trajectory was calculated for each release point every 6 hours, starting from August 1st at 00:00. In this configuration, ROTRAJ outputs the location, specific humidity, and temperature, extracted from the ERA5 reanalysis, at each time step along each trajectory.

We applied the same set of release points daily over the study period, and used the daily fire emission distribution to activate or deactivate the trajectories (i.e., to select which were included in the analysis for each day). Additionally, the emissions were used to weight trajectories to characterise the plume (see Section 2.4). For this, we use CO emissions from the near-real-time extension of the fifth version of the Global Fire Emissions Database (GFED5.1) (van der Werf et al., 2025). In South America, GFED5.1 has been shown to present higher CO emissions than other commonly used inventories, particularly in forest cover (Velásquez-García et al., 2026). However, more moderate inventories have been shown to underestimate emissions for this 2024 event by a factor of 1.5-3 (de Laat et al., 2026).

2.4 Biomass burning plume characterisation

The biomass burning plumes originating from South America were identified by combining the locations of the forward trajectories and the TCCO and TCHCOOH values above a subjective threshold ($2.0\times\ 10^{18}$ molecules cm^{-2} and $0.008\times\ 10^{18}$ molecules cm^{-2}, respectively). We chose the thresholds based on imagery observations of biomass burning plumes during the period (e.g., see Figs. S3 and S4). The chosen thresholds enable a more pronounced extraction of in-plume trace-gas enhancements, distinguishing them from background levels. The locations of the forward trajectories were gridded at the same spatial resolution as the satellite-retrieved data (i.e., $1.0^\circ\times1.0^\circ$ grid). The trajectory steps in a grid were aggregated daily as layers with all their features (i.e., temperature, humidity, altitude, and age). Only daily grids with a minimum overlap of five trajectory steps (a balance between sample size and the retention of spatial information) and with TCCO and TCHCOOH values exceeding the subjective thresholds were used, limiting the analysis to the more frequent transport route of the South American plumes and avoiding paths of solely African plumes.

The weighted median was used to represent the grid features in the multilayer grid. Here, we linearly weighted each trajectory step by age-adjusted emission strength, assuming that plumes with larger emissions would dominate the observed variability in satellite retrievals. The GFED5.1 CO emissions at the release point (t=0) were adjusted by trajectory age at each trajectory step to account for chemical loss and dispersion outside the plume. For every 3-hour step, the CO emissions (E, kg/kg) were reduced using an e-folding lifetime (τ) of 30 days (see Equation 1):

$$E_t = E_{t-1}e^{\Delta t/\tau} \tag{1}$$

Here, E_0 is the actual emission at the starting location; this is reduced by an e-folding lifetime, where Δt (seconds) is the 3 h step and τ (seconds) = 30 days. A 30-day lifetime is used, based on Goudar et al. (2023). Different weighted-average methods were analysed, yielding consistent results (see Figure S5(b)).

To investigate the spatio-temporal evolution of TCHCOOH, we employed the normalised enhancement ratio of TCHCOOH relative to TCCO (NER$_{HCOOH}$) and the direct ratio between the two products, TCHCOOH:TCCO. NER$_{HCOOH}$ is defined as

https://doi.org/10.5194/egusphere-2026-6903
Preprint. Discussion started: 12 November 2026
© Author(s) 2026. CC BY 4.0 License.

the slope obtained from a linear regression of TCHCOOH against TCCO, calculated within isolated biomass burning plumes for each estimated day of plume age. NER_{HCOOH} enables direct comparison with values reported in the literature and is also dilution-corrected by background removal. The TCHCOOH:TCCO ratio is used to compare observed data directly with HCOOH:CO ratios produced by the box model simulations. We evaluated different thresholds, as shown in Fig. S5(a), which produced a similar evolution of the TCHCOOH:TCCO ratio throughout the ageing plume, although variability was large at the oldest stage, resulting in different slopes. So, to capture the broader range of variation beyond the initially selected threshold, we included two additional alternative thresholds when calculating the trend slopes for both ratios. Specifically, we used nine combinations of the pair of thresholds based on 0.006, 0.008, and 0.01 $\times$ 10^{18} molecules cm^{-2} for TCHCOOH, and 1.8, 2.0, and 2.2 $\times$ 10^{18} molecules cm^{-2} for TCCO. For each threshold pair, we calculated the slopes using ordinary least squares regression, repeated within 1000 bootstrap iterations. We report the slope as the mean with a 95% confidence interval.

2.5 Box model analysis of in-plume HCOOH sensitivities

We use the box-model version of the UKCA scheme (O'Connor et al., 2014), the atmospheric chemical model of the United Kingdom Earth System Model (UKESM), to assess the chemical budget of HCOOH in biomass burning plumes. For this study, we refer to this box model as UKCA-box. Currently, UKCA-box is primarily used as a development tool for UKCA, as it omits key processes such as dry/wet deposition and emissions (Esentürk et al., 2018). However, because it runs the same UKCA code over a single cell, neglecting the impacts of atmospheric transport that would occur in UKESM, it can cost-effectively test the short-term temporal evolution of atmospheric chemistry within an atmospheric parcel using pre-defined initial conditions. For this study, we conduct a sensitivity analysis assessing the response of HCOOH to varying initial chemical conditions. We used the UKCA-box with the Common Representative Intermediates version 2.2 tropospheric chemistry mechanism, CRI v2.2, combined with stratospheric chemistry (CRI-Strat) (Archer-Nicholls et al., 2021). CRI-Strat is an intermediate-complexity chemistry scheme that represents the near-explicit mechanisms of the Master Chemical Mechanism while reducing its complexity via lumped species and reactions (Archer-Nicholls et al., 2021). Here, CRI-Strat is coupled to the GLObal Model of Aerosol Processes (GLOMAP) (Spracklen et al., 2005) to represent aerosol evolution. CRI-Strat + GLOMAP has more than double the number of reactions and almost three times the number of chemical species than the simplified Strat-Trop + GLOMAP scheme commonly used in UKESM (Archer-Nicholls et al., 2021). Although this makes using the CRI-Strat scheme more computationally expensive for a UKCA simulation, it is appropriate for sensitivity testing within a box model.

CRI-Strat contains four sources and one sink of HCOOH. As sources, it includes the OH-oxidation of C_5H_8, acetylene (C_2H_2), and hydroxymethyl-methyl-α-lactone ($C_4H_6O_3$, also known as HMML), as well as the ozonolysis of ethene (C_2H_4), the simplest alkene. HMML is produced in a downstream step of the C_5H_8 oxidation chain, triggered by the presence of NO (Daimari et al., 2026; Jenkin et al., 2015). In CRI-Strat, the HMML oxidation reaction is a lumped version of two explicit reactions in the Master Chemical Mechanism. In forested environments, C_5H_8 is recognised as a major precursor for HCOOH production (Link et al., 2020). In contrast, C_2H_2 is identified as a dominant non-biogenic precursor (Paulot et al., 2011). In the model, HCOOH is lost by OH-oxidation, and because the UKCA-box does not include any physical loss, this is the only sink of HCOOH considered in this study. However, because we focus on lofted plumes in the free troposphere due to the vertical

https://doi.org/10.5194/egusphere-2026-6903
Preprint. Discussion started: 12 November 2026
© Author(s) 2026. CC BY 4.0 License.

Table 1. Comparison of initial meteorological conditions and mass mixing ratio (MMR) for the UKCA box model control simulation and SAMBBA-obs experiment.

Meteorological variable	Control value	Initial MMR [kg/kg]	MMR control[a]	MMR SAMBBA-obs
Latitude [°]	−12	CO	2.82×10^{-7}	2.82×10^{-7}
Longitude [°]	−55	NO	3.96×10^{-11}	7.70×10^{-11}
Temperature [K]	291.64	NO_2	2.07×10^{-10}	5.20×10^{-10}
Pressure [hPa]	850	C_2H_6	9.6×10^{-9}	1.88×10^{-9}
Surface temperature [K]	299.62	O_3	1.05×10^{-7}	2.91×10^{-8}
Boundary layer height [m]	430.89	C_5H_8	4.5×10^{-11}	1.30×10^{-9}
Surface pressure [hPa]	975	C_2H_4	1.0×10^{-15}	2.67×10^{-9}
Water vapour in air [kg/kg]	0.007	C_3H_6	1.0×10^{-15}	1.52×10^{-9}
Cloud ice in air [kg/kg]	0	C_2H_2	1.0×10^{-15}	5.09×10^{-10}
Liquid cloud water in air	0	C_4H_{10}	1.0×10^{-15}	1.89×10^{-10}
Surface albedo	0.2	C_3H_8	3.02×10^{-9}	6.11×10^{-10}
		BENZENE	1.0×10^{-15}	1.62×10^{-9}
		TOLUENE	1.0×10^{-15}	9.24×10^{-10}

[a] 1.0E-15 is the default mass mixing ratio if no other initial condition is available for the compounds.

sensitivity of satellite retrievals, OH oxidation is expected to dominate over other sinks of HCOOH. Loss from dry and wet deposition is negligible and minor, respectively (Paulot et al., 2011; Franco et al., 2021). The UKCA-box does not include the proposed source of HCOOH from aerosol and cloud heterogeneous reactions (Franco et al., 2021; Jiang et al., 2023).

UKCA-box was setup to run a control 240 h (10 days) simulation at a location matching a central plume release point for ROTRAJ at 12°S, 55°W in mid-west Brazil, and an altitude of 850 hPa. We ran the UKCA-box starting at 9 am, close to the morning overpass time of MetOp. At this time (9 am), the results from the model were compared with satellite retrievals day by day. The initial conditions used in UKCA-box (chemical species mass mixing ratios - Table S1) were extracted for the same location on the 31st of August 2014 from a UKESM simulation, which used the UKCA Strat-Trop scheme with all atmospheric processes considered. This was the most relevant available dataset from a model simulation that used UKCA with both hourly resolution and including the fire season for South America. UKESM simulations incorporating UKCA have been shown to capture large-scale chemistry over fire-active regions. They demonstrate reasonable agreement with satellite observations of total column CO and NO_2 in areas of intense biomass burning (Archibald et al., 2020). Additionally, UKCA simulations compare well with aircraft measurements of organic aerosols during biomass-burning events (Kelly et al., 2019). For the box model, the initial meteorological conditions (Table 1) were obtained from the 2024 ERA5 reanalysis as extracted by ROTRAJ at the release location.

Two sensitivity experiments were conducted using UKCA-box, to compare with the control experiment described previously (summary in Table 1). The first experiment, designated “SAMBBA-obs”, aims to intialise the model from the closest possible

https://doi.org/10.5194/egusphere-2026-6903
Preprint. Discussion started: 12 November 2026
© Author(s) 2026. CC BY 4.0 License.

real state of atmospheric chemistry under biomass burning conditions. For this, SAMBBA-obs incorporates initial conditions for 13 chemical species based on aircraft observations from the South American Biomass Burning Analysis (SAMBBA) campaign, flight B737. This flight took place in Rondônia state in the Amazonian tropical forest in western Brazil on 20^{th} of September 2012 and targeted fresh biomass burning emissions (Hodgson et al., 2018). The measurements were taken at an altitude of around 780 hPa .To extract the in-plume observations, we used a CO threshold of 3.38 $\times 10^{-15}$ kg kg^{-1} (350 ppbv) (see Fig. S6). We extracted the mass mixing ratios from 12:00 to 13:00 UTC-4 (local time) when CO exceeded the threshold. These values were then averaged and scaled to enable direct comparison with the UKCA HCOOH and other simulated species in the control experiment. We scaled the SAMBBA-derived observations using the ratio between the UKCA CO and the SAMBBA mean CO (i.e., 2.82/6.58). The scaled mass mixing ratios for the 13 species extracted for this experiment are presented in Table 1 along with their counterpart used in the control run. The SAMBBA-extracted compounds include C_5H_8, C_2H_2, and C_2H_4, which can directly affect the HCOOH budget in UKCA-box. The second experiment, labelled as "SAMBBA-obs-noMPAN," aims to evaluate HMML-derived HCOOH formation, as HMML was not observed in the SAMBBA campaign, unlike the other HCOOH precursor species in the UKCA-box. In both the control and SAMBBA-obs, HMML is primarily produced by peroxymethacrylic nitric anhydride (MPAN), which in both experiments is initialised based on the extracted mass mixing ratios from the UKESM simulation. Therefore, SAMBBA-obs-noMPAN uses the same initial conditions as SAMBBA-obs for all chemical species except for MPAN. Here, we change the initialised MPAN concentrations from 2.97$\times 10^{-9}$ kg kg^{-1}, as used in the control experiment, to a lower-limit initial concentration of 1.0×10^{-15}.

3 Results and discussion

3.1 Fires in South America from August to October 2024

During the 2024 fire season in South America, significant active fires and CO emissions were predominantly detected in Brazil and Bolivia, as shown in Fig. 2 (a). Although the land area of Bolivia is approximately 13% of the area of Brazil, the total CO emissions from August to October 2024 were similar. Bolivia emitted around 54 Tg of CO, and Brazil around 57 Tg of CO. Lower, frequent and significant emissions were also detected in Paraguay, Perú, and Argentina. Fire activity was predominantly observed in forests and savannas, with a smaller fraction in grasses and croplands (see Fig. S9). We estimate that around 47% of derived hotspots were present on forest-dominated lands, including evergreen broadleaf forest, deciduous broadleaf forest, and evergreen needleleaf forest, with evergreen broadleaf forest accounting for the largest share of hotspots (34% of total hotspots). According to de Laat et al. (2026), forest fires, rather than deforestation fires, dominated CO emissions during the 2024 fire season in South America. The contribution of each land cover to the total number of hotspots fluctuated by around 10% throughout the study period, but the contributions remained relatively stable. Savanna-dominated land contributed around 35% of the total hotspots. According to Akagi et al. (2011), forest fires emit more CO and HCOOH than savanna fires, and the proportion of HCOOH relative to CO is also higher in forests. Based on the emission factors, the HCOOH:CO emission ratio is 8.5 $\times 10^{-3}$ g g^{-1} and 3.3 $\times 10^{-3}$ g g^{-1} for forest and savanna, respectively (Akagi et al., 2011). Over the study

https://doi.org/10.5194/egusphere-2026-6903
Preprint. Discussion started: 12 November 2026
© Author(s) 2026. CC BY 4.0 License.

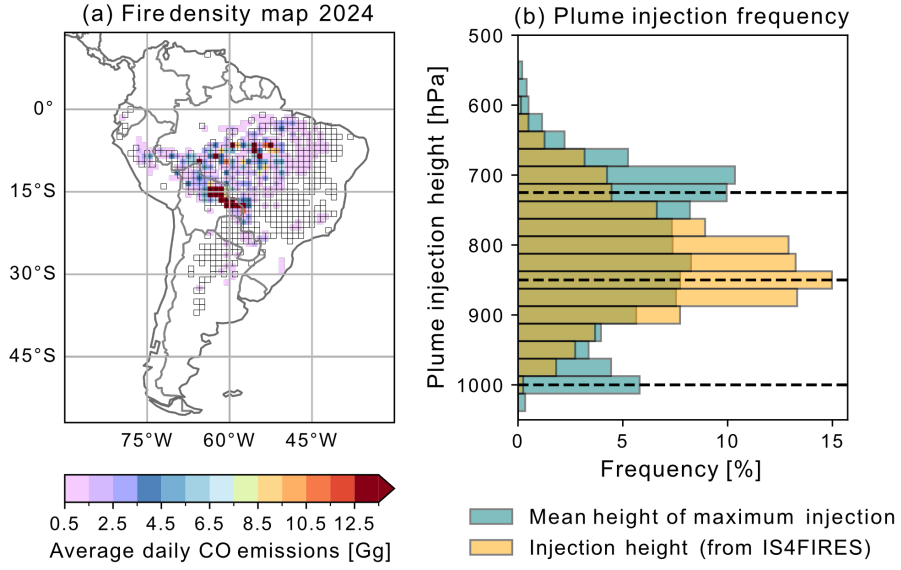


Figure 2. (a) Fire activity (black squares represent cells with dense hotspots with FRP > 100 MW) and CO emissions [Gg] (background colour). (b) Histogram of biomass burning plume injection altitude [hPa] based on the 1-D model and IS4FIRES products proposed by GFAS. In panel (b), the horizontal dashed lines describe the heights 725, 850, and 1000 hPa, observed as peak plume injection heights.

period, TCHCOOH and TCCO have a high correlation coefficient (r = 0.93), which provides evidence consistent with their co-emission.

According to the combined distribution of the plume injection height products in Fig. 2 (b), emissions were primarily released near the surface (around 1000 hPa) and at 850 and 700 hPa, corresponding to altitudes of approximately 130, 1500, and 3000 meters. This pattern aligns closely with the typical range of smoke transport. This is supported by Gonzalez-Alonso et al. (2019); Jury et al. (2021); Marenco et al. (2016), who describe a typical dense smoke layer near the surface and at around 900 and 600 hPa over the South American continent using CALIOP lidar data and an aircraft campaign. These altitudes (i.e., 1000, 850, and 700 hPa) were used to release the 10-day ROTRAJ forward trajectories. As expected for the region, the surface-released trajectories tended to accumulate over the continent, particularly to the east of the Andean Mountains. As a result, around 50% of the surface-released 10-day trajectories had a net horizontal distance between the release point and the endpoint of less than 5 degrees. In contrast, the median distances for the trajectories released at 850 and 700 hPa were 20° and 22°, respectively. We excluded surface-released trajectories from further analysis because they remained in the lower troposphere (median 995 hPa), whereas the satellite retrievals are most sensitive to the mid- and upper troposphere.

3.2 Biomass burning plume transport and features

Once we identified South American biomass burning plumes, we examined their transport patterns and characterised features. Figure 3 (a) and (b) illustrate the density of both the forward trajectories and pixels exceeding the satellite column thresholds.

https://doi.org/10.5194/egusphere-2026-6903
Preprint. Discussion started: 12 November 2026
© Author(s) 2026. CC BY 4.0 License.

In Fig.3 (b), the black contour line encircles the compiled daily accepted trajectory and threshold limits, indicating that plumes outside this area were not considered in the study. In Fig. 3 (b), the density of pixels exceeding the threshold during the study period shows two common paths for the plumes over the Atlantic Ocean, covering at least 20% of the study days. The paths connecting South America and Africa are below and above 10°S, each covering a latitude range of about 20° to the south and north, respectively. In Fig. 3(a), the trajectory model primarily simulates the southern path, suggesting this as the more frequent path for plumes originating in South America. Our observations show that the 10°S to 10°N latitude range is also frequent for South American plumes moving eastward in October (see Figs. S3 and S4). However, the frequency of days with threshold exceedance was above 50%, while only 10% of days had South American trajectories. This indicates that this latitudinal range was primarily associated with African plumes moving westward toward South America.

TCHOOH controls the daily data coverage because the weaker HCOOH spectral signature results in fewer robust retrievals than TCCO. Consequently, data coverage is further reduced in regions with persistent cloud cover and over highly reflective surfaces, where a larger proportion of observations fail the filtering criteria. In Fig. 3 (b), the areas lacking data point to highly reflective areas such as over the Sahara Desert and the western South Atlantic and South Pacific oceans, regions often covered by marine stratocumulus clouds.

Biomass burning plumes from South America reached both the Atlantic and Pacific oceans. According to the forward trajectories, around 64% of the plumes reached the Atlantic, while 17% reached the Pacific Ocean. In the studied period, the transport of large plumes of biomass-burning emissions across the continent was largely controlled by the South American Low-Level Jet (SALLJ) at the eastern flank of the Andean mountains (Forgioni et al., 2025). This, together with frequent biomass burning emissions, explains the high density of trajectories and younger-aged plumes across eastern Perú, Bolivia, and Paraguay. At around 25°S, the plume shifted eastward. This shift is possibly influenced by synoptic circulation configurations such as the "no Chaco jet event", a SALLJ phase. The no Chaco jet event is characterised by strong zonal winds eastward in mid-latitudes (Ramos et al., 2019).

Plume ages were characterised using the forward trajectory transport times since emission. Figure 3 (c) shows the average plume age through the sampled plume area. The method showed a consistent transition of plume age through transport, where older plumes are located farther from the emission source (see Figs. 3 (c), Fig. S7 and S8). In Fig. 3 (c), the eastern side of the Andes Mountains towards the Atlantic presents an interquartile range (IQR) of 3 days, probably as a consequence of accumulation. This includes Bolivia, which, despite having many fresh plumes, has a median age of 1 day. Bolivia lies within the area of effect of the SALLJ and in an accumulation zone because the Andean Mountains act as a natural barrier; therefore, it is a region of recurring circulation and a likely receptor of older plumes. On average, the freshest plumes (0 days) are in southeast Brazil, around 0°N and 50°W; fire occurrence was lower than in other regions (see Fig. 2), but as shown in Fig. 3 (a), it is not largely influenced by other plumes. Figure 3 (c) also represents well the time that biomass burning plumes take to reach key zones. Based on our findings, biomass burning plumes took, on average, about 4 days to reach the Atlantic Ocean and 6 days to reach the African continent. These ages match the estimates calculated by Tereszchuk et al. (2011) for the 2004 South American fire season. Under less favourable circulation conditions, biomass burning plumes took 5 days to cross the Andes, change hemispheres, and reach the Pacific Ocean.

https://doi.org/10.5194/egusphere-2026-6903
Preprint. Discussion started: 12 November 2026
© Author(s) 2026. CC BY 4.0 License.

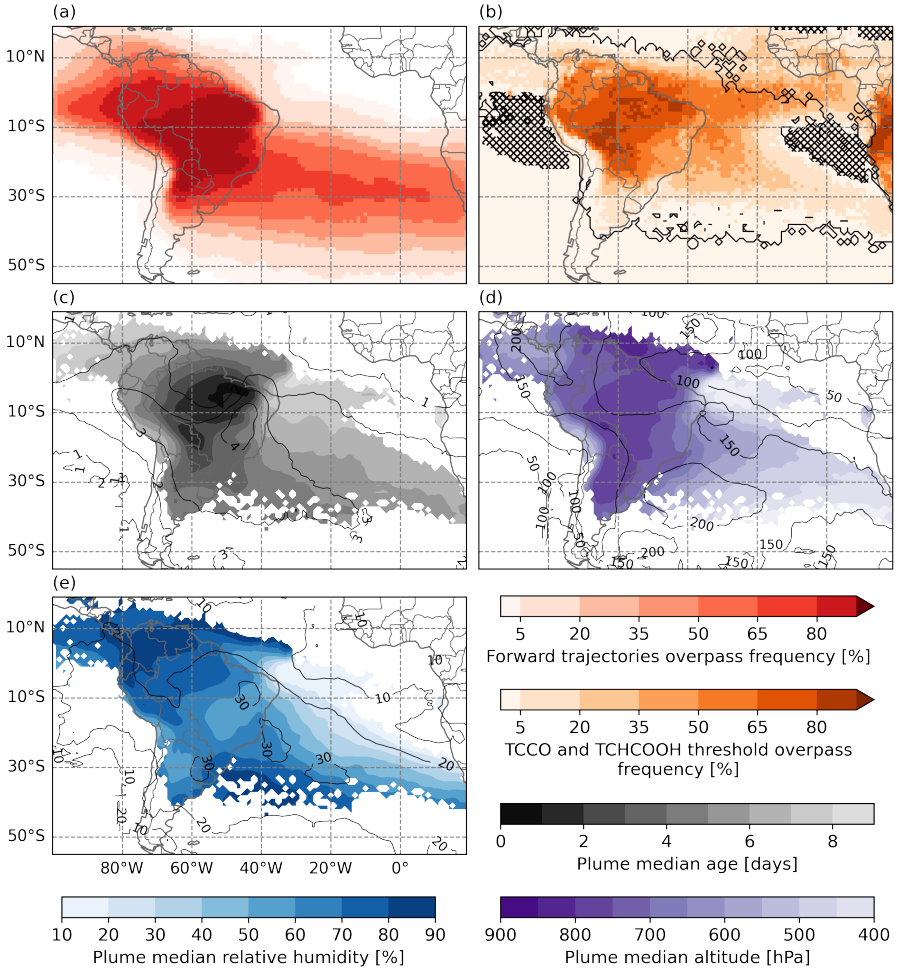


Figure 3. Biomass burning plume identification from South America using both (a) forward trajectory frequency and (b) observation over the set threshold (i.e., TCCO > 2.0 $\times 10^{18}$ molecules cm^{-2} and TCHCOOH > 0.008 $\times 10^{18}$ molecules cm^{-2}); and biomass burning plume characterisation based on (c) age (days), (d) altitude (hPa), and (e) relative humidity (%). The black contour in panel (b) represents the area of valid biomass-burning plumes for the study, whereas the black contours in panels (c)-(e) represent the interquartile ranges of the estimated features, with the same units as those presented in the background colour. In panel (b), the hatched area indicates the area with unavailable TCHCOOH data for the study.

The altitude and relative humidity of the biomass burning plumes were determined from ROTRAJ trajectories. According to the estimates shown in Fig. 3 (d), on average, the biomass burning plumes are transported at around 850-700 hPa over the continent, which, as mentioned in Section 3.1, aligns with the literature. In the Atlantic, the calculated transport altitude increases from 700 to 400 hPa, which also matches a previously observed biomass burning plume from South America crossing the Atlantic (Johansson et al., 2022). The plume moved over southern Africa at about 400 hPa, matching observations for South

https://doi.org/10.5194/egusphere-2026-6903
Preprint. Discussion started: 12 November 2026
© Author(s) 2026. CC BY 4.0 License.

American biomass burning plumes in 2022 (Ranaivombola et al., 2025). In Fig. 3 (e), relative humidity reaches its maximum levels over northern South America ($\sim$ 90%), due to the intertropical convergence zone location. The high humidity extends as SALLJ transports humidity to the south (relative humidity $>$ 60%). Large relative humidity is also observed in the colder south Atlantic. According to our estimates, the relative humidity within the biomass burning plumes was, on average, 62%, similar to the 60% reported by Guyon et al. (2005) from a biomass burning plume in the Amazon. This can still vary widely. The relative humidity estimated for biomass burning plumes has an absolute IQR of 23%.

Applying this trajectory approach enabled the assessment of plume feature variability by calculating a range of characteristics for each pixel traversed by multiple trajectories. This method captures the intricate nature of plume dynamics and demonstrates its robustness by producing features within the literature range. Previous studies have commonly used back-trajectory analyses because observational data are typically restricted to plume transects obtained from ground-based or airborne measurements (e.g., Alvarado et al., 2015; Chen et al., 2021; Permar et al., 2023). In the present study, forward trajectory modelling was more appropriate, given the large spatial scale of the event, persistent emission sources, and multiple fire hotspots. Still, methods for plume characterisation that consider multiple continuous biomass burning plumes should continue to be evaluated and refined to produce high-quality results that can inform future studies using combined datasets and models. As more retrievals are available, future research should explore and compare alternative approaches, such as applying photochemical ageing to estimate plume age, alongside traditional techniques to improve the accuracy and reliability of satellite-based analyses.

3.3 HCOOH evolution within the ageing plume

Having characterised key biomass burning plume features, we then assess how HCOOH levels evolve as the plumes age. Figure 4 shows the TCHCOOH:TCCO variability for each day during the first 10 days after emission. Daily TCHCOOH:TCCO ratios show moderate variability, with an IQR up to 40% of the median magnitude. Figure 4 also presents the calculated age IQR, with an average magnitude of 2.8 days. The TCHCOOH:TCCO on Day 0 has a median value of 5.5 $\times 10^{-3}$ and an IQR of 1.9 $\times 10^{-3}$. From Day 0, TCHCOOH:TCCO increases by around 5.7 $\pm$ 1.0% day^{-1} to Day 1 (median value 5.9 $\times 10^{-3}$). TCHCOOH:TCCO median magnitudes are similar ($<$2% variation) from Day 1 to Day 2. After this, the TCHCOOH:TCCO ratio at a faster rate when including plumes transported over the ocean than when considering only those on the continent (see Fig. 4). From Day 2 to 6, the total set of plumes analysed decays at a rate of 4.8 $\pm$ 0.8 % day^{-1}, while those transported solely over the continent decay at a rate of 3.8 $\pm$ 1.1 % day^{-1}. After Day 6, the set of all plumes continues to decay more slowly, at 2.1 $\pm$ 1.0 % day^{-1}. In contrast, those transported only over the continent stabilise with a non-significant slope trend of -0.7 $\pm$ 1.4 % day^{-1}.

The difference in the magnitude and temporal evolution of species in the biomass burning plumes likely depends on the background state. Continental-only plumes will have elevated background concentrations due to fresh and recirculated plumes, as well as fresh emissions from other sources (e.g. HCOOH precursors emitted from vegetation). Continent-Ocean plumes will typically have a lower background given the relatively clean ocean state the plumes propagate over in the latter stages of the plume life cycle. However, the NER$_{HCOOH}$ metric (which accounts for the background state) declines at a similar rate independent of plume location(see Table 2 and Fig. S12). By accounting for the background influence, the NER$_{HCOOH}$ has a

https://doi.org/10.5194/egusphere-2026-6903
Preprint. Discussion started: 12 November 2026
© Author(s) 2026. CC BY 4.0 License.

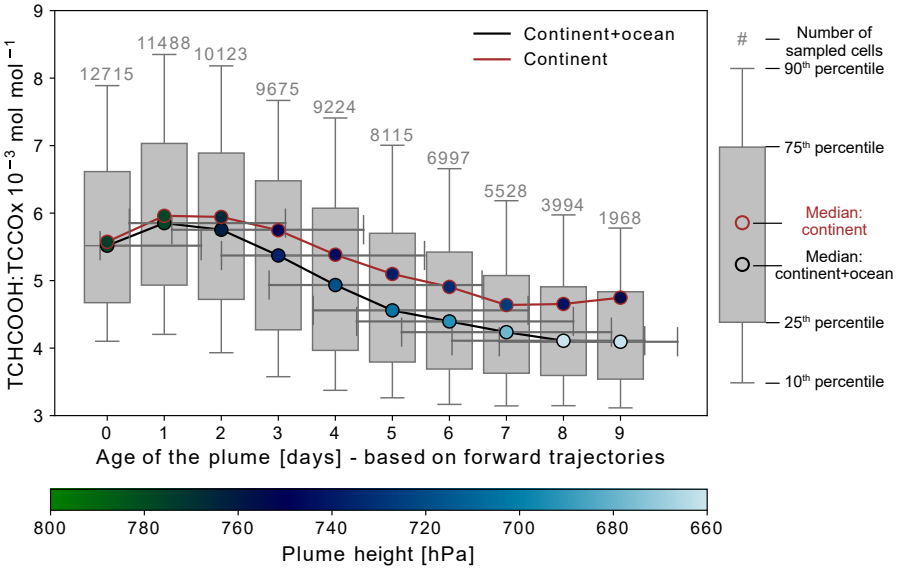


Figure 4. Box plot of the TCHCOOH:TCCO ratio by day of age for biomass-burning plumes. The black line describes the median magnitude of all characterised plumes at each age, while the dark red line considers only plumes over continental South America (i.e., excluding plumes over the ocean). The filled circles indicate the average plume height [hPa] for each dataset on the given colour scale.

steeper decline (-9.2± 0.1 % day^{-1}) than the direct TCHCOOH:TCCO ratio (i.e. the background remains within the column quantity when the ratio between pollutants is calculated). Additionally, according to NER$_{HCOOH}$, continent-only plumes may show significant HCOOH formation after Day 1, continuing until Day 4, which is obscured in the TCHCOOH:TCCO evolution and contributes to a smaller decay of TCHCOOH:TCCO over the continent. This sustained formation may reflect more frequent entrainment of HCOOH precursors from other plumes and/or biogenic and urban-sourced compounds over the continent. Additionally, as Figs. 4 and S13 show, plumes transported over the ocean tend to be lofted to higher altitudes, where temperature decreases, and HCOOH and/or its precursors might partition to the particle phase (Morgan et al., 2010; Lv et al., 2022), causing NER$_{HCOOH}$ to decline more quickly. Overall, the evolution of the TCHCOOH:TCCO ratios in continental plumes is particularly complex, as it reflects a more heterogeneous background.

NER$_{HCOOH}$ in Table 2 follows a similar pattern to TCHCOOH:TCCO but shows pronounced changes, which in general agree with the literature. On Day 0, the NER$_{HCOOH}$ ratio was 6.6 × 10^{-3} mol mol^{-1}, which is in acceptable agreement with previous observations of South American biomass burning, as presented in Table 2. The literature has consistently provided evidence of strong formation of HCOOH in the biomass burning plumes during the first hours after emission (Alvarado et al., 2015; Permar et al., 2023; Yokelson et al., 2009), which aligns in direction with the observed enhancement of TCHCOOH:TCCO and NER$_{HCOOH}$ on Day 1 in Fig. 4 and Table 2, respectively. From aircraft measurements in fresh plumes, Alvarado et al. (2015); Permar et al. (2023) reported that NER$_{HCOOH}$ doubles its magnitude within a few hours. Here, using satellite observations, we calculate an 8.4± 0.1% day^{-1} increase in the NER$_{HCOOH}$ on the first day after emission. Because

https://doi.org/10.5194/egusphere-2026-6903
Preprint. Discussion started: 12 November 2026
© Author(s) 2026. CC BY 4.0 License.

Table 2. Normalised enhancement ratio of HCOOH relative to CO (NER_{HCOOH})[mol mol^{-1}] with its confidence intervals[a] and extracted from the literature for South America.

Age	This study		Literature		
	NER_{HCOOH} $\times 10^3$	r	NER_{HCOOH} $\times 10^3$	Reference	Instrument
0 days	6.6 ± 1.3	0.71	7.3 ± 0.1	Pommier et al. (2017)	IASI
			6.7 ± 2.1	Chaliyakunnel et al. (2016)	TES[b]
			5.1 ± 1.5	Abad et al. (2009)	ACE-FTS[c]
1 days	7.1 ± 1.5	0.79	152.6 ± 16.2	Chen et al. (2021)	ATom[d]
2 days	7.3 ± 1.5	0.77			
3 days	6.4 ± 1.4	0.69			
4 days	5.8 ± 1.3	0.62			
5 days	5.0 ± 1.3	0.56			
6 days	3.9 ± 1.3	0.49	2.6 ± 0.5	Tereszchuk et al. (2011)	ACE-FTS[c]
6–9 days	3.9 ± 0.8	0.51			

[a] confidence intervals calculated based on the standard Ordinary Least Squares confidence interval method.
[a] TES- Tropospheric Emission Spectrometer satellite sensor.
[b] ACE-FTS - Fourier transform infrared spectroscopy (FTS) in the satellite Atmospheric Chemistry Experiment (ACE).
[c] ATom - Atmospheric Tomography Mission aircraft campaign.

this study focuses on plumes transported at 850 hPa and above (i.e., higher altitude but lower pressure), large HCOOH losses are suggested along the route, particularly in the boundary layer (Chaliyakunnel et al., 2016), which might explain the discrepancies. At the same time, key HCOOH precursors might have decreased through lifting because semi-volatile gas-phase species partitioned to the particle phase at reduced temperatures (Morgan et al., 2010), especially under the humid conditions above the emission region (Darbyshire et al., 2019). Moreover, our analysis spans large spatial and temporal scales, so we consider different land cover, ignition conditions, and chemical pathways together, among other factors. Still, the Spearman correlation between TCHCOOH and TCCO, ranging from 0.5 to 0.8 across plume ages (see Table 2 and Fig. S10), suggests that our method robustly describes HCOOH evolution in the plume. Consistently, the correlation tends to decrease with plume age, as other physical (e.g., deposition) and chemical (e.g., oxidation) processes influence HCOOH in a different way than CO.

Beyond the day, few studies have tracked and characterised HCOOH in the biomass burning plume. Similar to this study, but based on fractions of varied plume origin and using aircraft measurements, Chen et al. (2021) showed a general decrease in the NER_{HCOOH} ratio from the first five days after emissions to the following five days of about 47% (from $38 \pm 12 \times 10^{-3}$ to $20 \pm 18 \times 10^{-3}$). When averaging the NER_{HCOOH} values in these clusters (i.e., from Days 0 to 4 and from Days 5 to 9), we report a similar estimate of 40% reduction. Although NER_{HCOOH} from Chen et al. (2021) for a South American fire (see

https://doi.org/10.5194/egusphere-2026-6903
Preprint. Discussion started: 12 November 2026
© Author(s) 2026. CC BY 4.0 License.

Table 2) is larger in magnitude, likely due to high boundary-layer values, the general temporal evolution of the plume shows similar behaviour. Likewise, as Tereszchuk et al. (2011) found in a Canadian Boreal plume, we estimated a decrease of around 20% in the NER_{HCOOH} from Days 0 to 1 to Days 4 to 5 based on satellite retrievals.

3.4 Box model simulation of HCOOH

We used the UKCA-box model to estimate the underlying sources and sinks of HCOOH in South American biomass-burning plumes and compared its evolution to satellite-derived estimates. Figure 5 (a) presents the control base simulation of the HCOOH:CO ratio using the CRI-STRAT chemical mechanism. The HCOOH:CO ratio falls within the IQR of the observed TCHCOOH:TCCO for the 10-day simulation. The initial HCOOH:CO magnitude (6.4 $\times 10^{-3}$) from which the simulation evolved was above the median observed ratio but still within the IQR. As illustrated in Fig. 5 (b), two reactions dominate the production and loss of simulated HCOOH in this control run: its formation via OH-oxidation of HMML and its loss via OH-oxidation (the only chemical sink in the model). The formation of HCOOH by HMML oxidation is limited to the first $\sim$three days after emission as HMML depletes. For Day 0 at midday, the HMML-derived flux was 4.5 $\times 10^4$ molecules of HCOOH $cm^{-3}\, s^{-1}$, while the OH-oxidation flux was 7.5 $\times 10^4$ molecules of HCOOH $cm^{-3}\, s^{-1}$. For Day 2 at midday, the HMML mixing ratio has decreased by approximately 76% relative to Day 0 (see Fig. 5 (a)), decreasing the sink flux by 89%. For sinks, OH decreased by 24% from Day 0 to Day 2 at midday, reducing HCOOH oxidation by 42%. OH oxidation was more consistent throughout the 10-day simulation. After three days from emission, the OH mass mixing ratio reaches an hourly maximum of $\sim 1.8 \times 10^{-13}$ kg kg^{-1} every day, as illustrated in Fig. 5 (a). As shown by this figure, OH, formed primarily by photolysis, exhibits a strong diurnal cycle that clearly influences the diurnal variability of products formed from its reactions.

Although the UKCA-box chemical scheme CRI-STRAT considers other reactions as HCOOH sources, their flux is three orders of magnitude lower than the HMML reaction in this simulation, as observed from 5 (b). The contribution of these reactions is limited by the initial mass mixing ratio of C_5H_8, C_2H_4, and C_2H_2, which, according to SAMBBA observations, might be at least two orders of magnitude larger than initialised in the control run (see Table 1). With the considered sinks and sources, HCOOH:CO constantly decrease at a rate of 3.6% day^{-1}. Even when HCOOH is produced in the first days of the simulation, the sink exceeds production.

The SAMBBA-obs experiment initialised the model with observed mass mixing ratios for several compounds, including C_5H_8, C_2H_4, and C_2H_2, that are much larger than in the control experiment (see Table 1). Figure 6 (a) shows that sources of HCOOH derived from C_2H_4 and C_2H_2 now play a significant role in the HCOOH budget, approaching the flux from HMML reaction. On Day 0 at midday, their reaction fluxes were at least 2 $\times 10^4$ molecules of HCOOH $cm^{-3} s^{-1}$, and after Day 2, C_2H_2 became the dominant source as all reaction rates declined. Similarly to the satellite-based analysis, SAMBBA-obs results show a slight increase in the HCOOH:CO ratio ($\sim$4.4%) from Day 0 to Day 1. However, it did not simulate the large formation of HCOOH in the first hours reported by previous studies (Alvarado et al., 2015; Permar et al., 2023). This may be explained by missing HCOOH sources, such as heterogeneous reactions and/or missing gas-phase reactions. According to the budget, at midday on Day 0, reactions involving C_2H_4 and C_2H_2 account for about 37% and 24% of the HCOOH, respectively, while the HMML reaction also explains about 37%. The contribution from C_5H_8 drops from 20% to below 1% in the first five

https://doi.org/10.5194/egusphere-2026-6903
Preprint. Discussion started: 12 November 2026
© Author(s) 2026. CC BY 4.0 License.

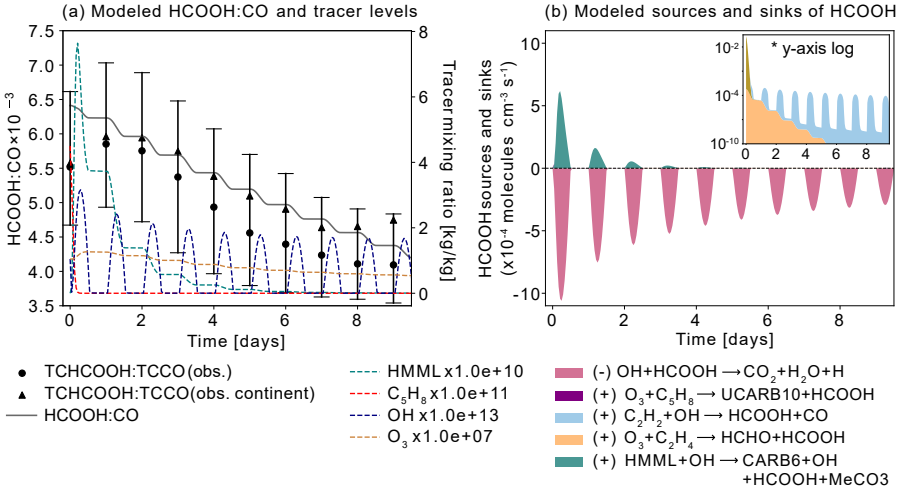


Figure 5. UKCA-box 10-day simulation of (a) HCOOH:CO and species related to HCOOH chemistry, and (b) simulated sources and sinks of HCOOH. Panel (a) contains the ratio of the total column HCOOH:CO for the complete dataset (black circles and whiskers) and the continent-only observations (back triangles).

hours as its mass mixing ratio decreases by 99%. During the night, C_2H_4 explains almost all HCOOH formation, since O_3 remains available (see Fig. 5). However, C_2H_4 is depleted within the first three days, consistent with previous biomass-burning measurements Johansson et al. (2022). This nighttime contribution is particularly important for the increase in the HCOOH mass mixing ratio on Day 1 (see Fig. S14).

After Day 1, in SAMBBA-obs, the HCOOH:CO ratio declined at a rate of 2.7% day^{-1} to the end of the simulation. For Day 2, C_2H_4, C_2H_2 and HMML reactions have decreased by 94%, 46%, 81%, respectively, compared with Day 0. For midday on Day 2, the contribution of HMML reactions has dropped to ∼30%, while C_2H_2 reactions account for 60%. The formation of HCOOH from the C_2H_2 reaction is maintained at the same order of magnitude until the end of the simulation. For this experiment, the simulated ratio remained within the observed IQR until Day 4, exceeding it thereafter. This might be because of the missing physical sinks; however, excess production, perhaps from C_2H_2, is also a possibility. In general, although the decline rate in the control experiment seems to better represent the decay ratio of HCOOH, SAMBBA-obs support net HCOOH formation from Day 0 to 1, as described by the satellite-derived analysis, and point to likely main sources.

From the SAMBBA-obs-noMPAN run, we found that C_5H_8 alone is unlikely to produce the HMML needed to contribute significantly to HCOOH; instead, already oxidised products are required. Figure 6 (b) shows that reducing initial MPAN in the SAMBBA-obs-noMPAN experiment almost completely suppressed HMML contribution to HCOOH formation. Only small amounts of HMML were produced from the available C_5H_8, even under NO_x-saturated plume conditions that enhanced MPAN formation. As a result, whereas the control experiment and SAMBBA-obs. reached an hourly HMML maximum of ∼7.0 10^{-10} kg kg^{-1} on the first day, SAMBBA-obs-noMPAN peaked at only 2.0 10^{-11} kg kg^{-1}. The initial MPAN mass mixing ratio used for the other experiments, taken from the UKESM simulation, likely represents convective transport of oxidised products

https://doi.org/10.5194/egusphere-2026-6903
Preprint. Discussion started: 12 November 2026
© Author(s) 2026. CC BY 4.0 License.

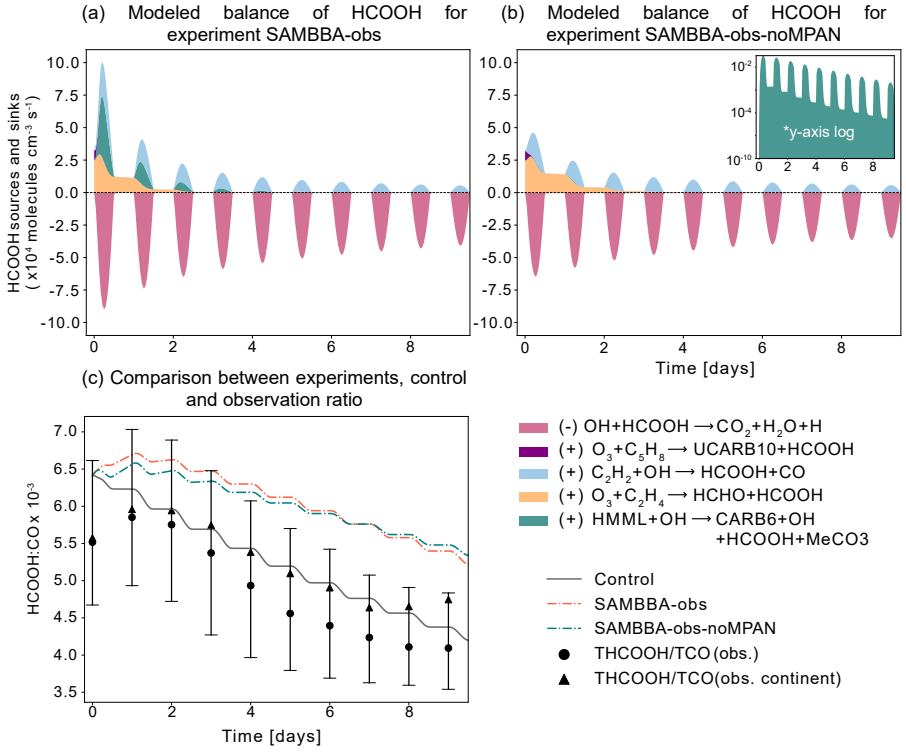


Figure 6. UKCA-box 10-day simulated sources and sinks of HCOOH for (a) SAMBBA-obs and (b) SAMBBA-obs-noMPAN experiments, and (c) HCOOH:CO ratio comparison for the control and experiment simulations, and observations. Panel (c) contains the ratio of the total column HCOOH:CO for the complete set of data (black circles and whiskers) and the continent-only observations (black triangles).

from vegetation-emitted C_5H_8 rather than from biomass burning. As Santos et al. (2018) suggested, C_5H_8 and its oxidation products in the plume come not only from biomass burning but also from vegetation emissions introduced via fire-induced convection. The quantitative contribution of HMML to HCOOH formation remains to be thoroughly evaluated, as it may substantially affect the initial HCOOH budget within the plume, particularly during forest fire events. Notably, even without significant HMML input in this experiment, the HCOOH:CO ratio increased by 2.4% from Day 0 to Day 1. After Day 1, this ratio declined more gradually than in the other experiments, at about -2% day^{-1}.

In general, experiments using the UKCA-box to simulate HCOOH:CO evolution show that fire emissions of C_2H_4 and C_2H_2 are key precursors of HCOOH, as well as HMML, which may came from biogenic emissions beyond biomass burning. However, the experiments slightly underestimated the increase in HCOOH after the emission day, likely because of missing HCOOH sources. The UKCA-box includes only gas-phase reactions and may still be missing key precursors. Although some other precursors have been reported, not all are well quantified, making it difficult to add them to a model (Millet et al., 2015). A missing source is HCOOH formation from formaldehyde (HCHO), which may be particularly important for this study because HCHO is expected to be highly abundant in the plumes (Kluge et al., 2020) and because the plumes reach high altitudes, where

https://doi.org/10.5194/egusphere-2026-6903
Preprint. Discussion started: 12 November 2026
© Author(s) 2026. CC BY 4.0 License.

the contribution of HCHO might be significant. Luo et al. (2023) suggest that the reaction of the Criegee intermediate (CH_2OO) with HCHO is a significant source of HCOOH in the upper troposphere. Based on different reaction pathways, Millet et al. (2015) also suggest the formation of HCOOH from HCHO and CH_2OO as a potential source in the upper troposphere. (Franco et al., 2021) suggested that hydrated HCHO could also form HCOOH through multiple pathways.

Expanding this research to different geographic regions is warranted, as our results already suggest significant regional differences. For example, HCOOH evolution in ageing plumes may vary with dominant land cover, as HMML may be strongly influenced by biogenic emissions. Also, the distinct levels of C_2H_2, C_2H_4, and C_5H_8 between regions, such as those observed in South America and Africa (Blake et al., 1996), likely influence HCOOH evolution in the ageing plume. Using more spatially and chemically complex models that incorporate dynamic losses and heterogeneous mechanisms proposed in the literature could further strengthen the analysis.

3.5 Potential Impact of aerosols on HCOOH abundance within the biomass burning plume

Recent studies have suggested that heterogeneous reactions on aerosols may contribute significantly to the production of HCOOH in both ambient conditions (Jiang et al., 2023), and biomass-burning plumes (Zhang et al., 2025). However, this potential source has not yet been incorporated into UKCA and is therefore not considered in UKCA-box simulations (Section 3.4). Nonetheless, to elucidate the potential influence of aerosols, we used MODIS AOD as a proxy for aerosols and compared its variability relative to CO (i.e., AOD:TCCO) with TCHCOOH:TCCO. Figure 7 (a) presents the correlation coefficient between TCHCOOH:TCCO and AOD:TCCO under all conditions and different relative humidity conditions, as this might condition the influence of aerosols (Zhang et al., 2025). We calculated the correlation in the full study area and specific sub-domains to mitigate potential spatial biases (e.g., between source and non-source areas). The correlation is moderate over the continent ($r>0.5$) and low over the ocean. In four out of the five domains (including the general domain), the correlation between TCHCOOH:TCCO and AOD:TCCO is larger when relative humidity is over 50%. Still, an exception is observed for the Brazil domain, which shows a high correlation of 0.68 under drier conditions. In the full domain, the correlation is ~ 0.5 only for Days 1 to 3; older ages present lower correlation.

This analysis does not suggest any causality. However, these positive correlations align with previous research on the heterogeneous formation of HCOOH on aerosol surfaces (Zhang et al., 2025; Jiang et al., 2023). Jiang et al. (2023) evidenced a strong positive correlation between HCOOH concentrations and aerosol abundance, especially in the fine size fraction and corroborated the signal with laboratory experiments. Furthermore, our findings support evidence that heterogeneous reactions produce higher HCOOH levels under wet conditions (Zhang et al., 2025), except for the Brazil sub-domain. The increasing correlation may reflect enhanced AOD from water uptake (Myhre et al., 2007), which triggers HCOOH formation via aqueous reactions at the aerosol interface (Cope et al., 2021). Still, HCOOH and secondary aerosols may form simultaneously from separate or common precursor compounds. For instance, HMML, a key precursor in UKCA-box simulations of HCOOH, also contributes significantly to secondary aerosol formation (Nguyen et al., 2015). However, contrary to our results, HMML-derived secondary organic aerosol formation is larger under dry conditions (Nguyen et al., 2015). In general, although our results are consistent with possible HCOOH formation via heterogeneous chemistry, the evidence here is insufficient and requires further research.

https://doi.org/10.5194/egusphere-2026-6903
Preprint. Discussion started: 12 November 2026
© Author(s) 2026. CC BY 4.0 License.

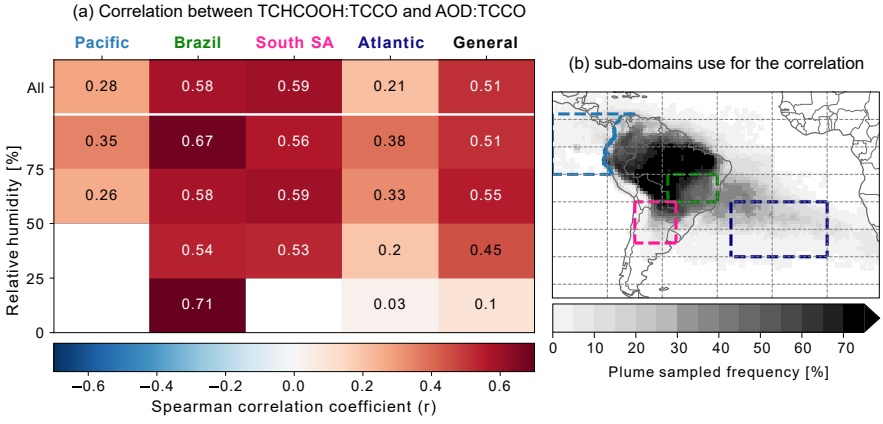


Figure 7. (a) Spearman correlation coefficient between the TCHCOOH:TCCO and AOD:TCCO ratios in different relative humidity conditions and in different sub-domains, which are shown in panel (b). The general study domain includes samples inside and outside the study domains. Panel (b) presents the spatial frequency of the available samples and the sub-domains used.

4 Conclusions

This study evaluated HCOOH evolution during ageing of South American large-scale biomass burning plumes during the 2024 fire season, using satellite-derived products. We used fire activity, CO emissions, and plume injection height estimates to simulate 10-day forward trajectories and characterise biomass burning plumes originating in the region. The trajectory release altitudes, based on CAMS estimates, were within the observed altitude range of biomass burning plumes transported over the continental region (i.e., near the surface and around 850 and 700 hPa). Only the higher injection heights were used, as the surface plume tended to stay at the surface, and satellite sensitivity constrains this study to plumes close to the mid-troposphere. We then identify the South American plumes, using both these trajectories and TCCO and TCHCOOH subjective thresholds. The plumes were characterised by age, altitude, and relative humidity using the trajectories and information extracted from ERA5 reanalyses. The age and altitude of the plumes across the South American continent, the Atlantic Ocean, and those reaching Africa matched features previously reported in the literature. During the study period, the latitude range between 30°S and 10°S was the most frequent transport pathway for South American plumes, while 10°S to 10°N was less frequent but a greater favourite for African plumes. On average, the plumes reach the Atlantic Ocean after four days, and some reach Africa after six days.

We quantified HCOOH in the plumes using two metrics: the normalised enhancement ratio relative to CO (NER_{HCOOH}) and the TCHCOOH:TCCO ratio. From Day 0 (day of emissions) to Day 1, both NER_{HCOOH} and TCHCOOH:TCCO increased by approximately $8.4 \pm 0.1\%$ day^{-1} and $5.7 \pm 1.0\%$ day^{-1}, respectively, suggesting net HCOOH production during the first day of transport. These rates match earlier reports of rising HCOOH in fresh biomass burning plumes. However, some studies report that atmospheric HCOOH concentrations can double within hours of emission. This rapid increase may reflect observational domains that encompass the lower troposphere, where compound abundances and dynamics are larger; however,

https://doi.org/10.5194/egusphere-2026-6903
Preprint. Discussion started: 12 November 2026
© Author(s) 2026. CC BY 4.0 License.

the total column estimate partially dilutes this effect. The large HCOOH abundance in the plume persists for another 1 to 3 days. Continent-only plumes tend to show steady NER_{HCOOH} values from Day 1 to 4, producing a smoother decline in TCHCOOH:TCCO than when including the plumes transported over the ocean. This may reflect entrainment of precursors from inland emissions; however, plumes rising through the troposphere and transported across the ocean might present greater VOC loss into the particular phase, leading to a sooner decline in NER_{HCOOH} and a steeper decline in TCHCOOH:TCCO when included. Both ratios stabilised by Day 8.

Simulations using the UKCA box model (UKCA-box), initialised from observations, agreed well with our satellite-derived estimates, showing an approximate 4.4% increase from Day 0 to Day 1. However, it did not capture the reported substantial increase in the HCOOH:CO ratio within the first hours, as reported in the literature; it did agree with our estimates. According to the UKCA-box observation-based simulation, HCOOH production on the first day after emissions was driven primarily by the oxidation of C_2H_4, HMML (a downstream oxidised product of C_5H_8), and C_2H_2. This HMML-derived formation warrants further analysis, as our literature review indicates it has not been reported in biomass burning plumes. Our experiments suggest that the C_5H_8 concentration in the plume may not be sufficient to produce the HMML concentration needed to contribute significantly to HCOOH formation. Instead, fire-induced convection of vegetation-emitted C_5H_8, along with oxidised compounds, might be a plausible source. This also makes HMML particularly relevant for forest fires. According to the simulation, on Day 2, C_2H_4 and HMML dropped by at least 81%, and the C_2H_2 reaction increasingly drove HCOOH sources, while the OH-oxidation sink dominated. The observation-based simulation underestimated the decline rate; however, this was better captured by a simulation initialised using the UK Earth System Model, which generally has lower VOC abundance.

The UKCA-box model does not account for heterogeneous reactions involved in HCOOH production. However, given their widely recognised importance in the literature, we examined the possible influence of such reactions occurring on aerosol surfaces using a simplified approach. We evaluated the correlation between THCOOH:TCCO and AOD:TCCO (which serves as a proxy for aerosol presence) under varying humidity levels and at different plume ages. In agreement with previous studies, we found a positive but weak correlation (Spearman r: 0.5–0.7), particularly within the first three days of plume transport and under more humid conditions. These findings support the hypothesis that heterogeneous reactions on aerosol surfaces contribute to HCOOH formation via aqueous-phase processes. Nevertheless, our analysis does not provide definitive evidence for the role of heterogeneous reactions, but it aligns with previous studies on this topic.

This study advances our understanding of HCOOH and the chemical evolution, transport, and atmospheric impact of biomass burning plumes, particularly on the week-long scale. Here, we show that satellite retrievals provide valuable complementary data for understanding biomass burning plume chemistry. This is especially important given the increasing frequency of large fire events worldwide and upcoming technological advancements that support mitigation and forecasting of fire atmospheric effects. Notably, the IASI New Generation instrument (IASI-NG) and the geostationary InfraRed Sounder (IRS) aboard the Meteosat Third Generation Sounder 1 (MTG-S IRS) will play key roles in these efforts. Studies like this one present different methodologies for analysing not only HCOOH but also other gases, while highlighting the underexploited capability of satellite data for weekly-scale analysis of atmospheric chemistry in biomass burning plumes.

https://doi.org/10.5194/egusphere-2026-6903
Preprint. Discussion started: 12 November 2026
© Author(s) 2026. CC BY 4.0 License.

Further investigation with satellite retrievals is needed to advance our understanding of atmospheric chemistry. To improve multi-satellite analyses, future research should develop new methods that address differences in vertical sensitivity and uncertainty when combining data from multiple satellites.

Code and data availability. The data of the IASI retrieval product total columns CO is available from Moore and Remedios (2025) at https://dx.doi.org/10.5285/4b31d47716604b9f84714fab39ce973c [last access: 06 November 2026]. The ULIRS team provided the HCOOH retrieval dataset, and you can request it by email (David P. Moore, dpm9@leicester.ac.uk). We downloaded the Porto Velho HCOOH estimates from Vigouroux et al. (2021). The Aerosol Optical Depth retrieved from MODIS can be found from NASA (2021) at https://catalogue.ceda.ac.uk/uuid/f5e2886edf254a42804b9a77af6d5c9c/ [last access: 06 November 2026]. ROTRAJ guideline can be found at https://www.met.reading.ac.uk/~swrmethn/ROTRAJ/ [last access: 06 November 2026]. The Met Office UKCA box model code is available for use under licence. For further information on how to apply for a licence, see https://www.metoffice.gov.uk/services/government/defence-and-security/code [last access: 06 November 2026]

Author contributions. All the authors participated in reviewing and editing this manuscript. Additionally, MPV: conceptualisation; data curation; formal analysis; investigation; methodology; software; visualisation; writing (original draft). RJP: conceptualisation; investigation; software; methodology; supervision; project administration. STT and SRA: conceptualisation; investigation; methodology; supervision; project administration. DPM: resources; formal analysis. RMD and AMG: methodology. MPC: project administration.

Competing interests. The corresponding author has declared that none of the authors has any competing interests.

Acknowledgements. Satellite retrieval access and pre-processing were performed using JASMIN, the UK collaborative data analysis environment (https://www.jasmin.ac.uk, last accessed: 19 August 2026). The box model experiments were performed using the MONSooN system, a collaborative facility supplied by the UK Met Office. This study was funded as part of the UK Research and Innovation Natural Environment Research Council's support of the National Centre for Earth Observation, grant nos. NE/X019071/1 and NE/R016518/1; and the Natural Environment Research Council, grant no. NE/S007458/1. The contributions of Steven Turnock were funded by the Met Office Climate Science for Service Partnership (CSSP) Brazil project under the International Science Partnerships Fund (ISPF).

https://doi.org/10.5194/egusphere-2026-6903
Preprint. Discussion started: 12 November 2026
© Author(s) 2026. CC BY 4.0 License.

References

Abad, G. G., Bernath, P. F., Boone, C. D., McLeod, S. D., Manney, G. L., and Toon, G. C.: Global distribution of upper tropospheric formic acid from the ACE-FTS, Atmospheric Chemistry and Physics, 9, 8039–8047, https://doi.org/10.5194/ACP-9-8039-2009, 2009.

Akagi, S. K., Yokelson, R. J., Wiedinmyer, C., Alvarado, M. J., Reid, J. S., Karl, T., Crounse, J. D., and Wennberg, P. O.: Atmospheric Chemistry and Physics Emission factors for open and domestic biomass burning for use in atmospheric models, Atmos. Chem. Phys, 11, 4039–4072, https://doi.org/10.5194/acp-11-4039-2011, 2011.

Alvarado, M. J., Lonsdale, C. R., Yokelson, R. J., Akagi, S. K., Coe, H., Craven, J. S., Fischer, E. V., Mcmeeking, G. R., Seinfeld, J. H., Soni, T., Taylor, J. W., Weise, D. R., and Wold, C. E.: Investigating the links between ozone and organic aerosol chemistry in a biomass burning plume from a prescribed fire in California chaparral, Atmos. Chem. Phys, 15, 6667–6688, https://doi.org/10.5194/acp-15-6667-2015, 2015.

Andreae, M. O., Talbot, R. W., Andreae, T. W., and Harriss, R. C.: Formic and acetic acid over the central Amazon region, Brazil 1. Dry season, Journal of Geophysical Research, 93, 1616–1624, https://doi.org/10.1029/JD093ID02P01616;ISSUE:ISSUE:DOI, 1988.

Archer-Nicholls, S., Abraham, N. L., Shin, Y. M., Weber, J., Russo, M. R., Lowe, D., Utembe, S. R., O'Connor, F. M., Kerridge, B., Latter, B., Siddans, R., Jenkin, M., Wild, O., and Archibald, A. T.: The Common Representative Intermediates Mechanism Version 2 in the United Kingdom Chemistry and Aerosols Model, Journal of Advances in Modeling Earth Systems, 13, e2020MS002 420, https://doi.org/10.1029/2020MS002420, 2021.

Archibald, A. T., O'connor, F. M., Abraham, N. L., Archer-Nicholls, S., Chipperfield, M. P., Dalvi, M., Folberth, G. A., Dennison, F., Dhomse, S. S., Griffiths, P. T., Hardacre, C., Hewitt, A. J., Hill, R. S., Johnson, C. E., Keeble, J., Köhler, M. O., Morgenstern, O., Mulcahy, J. P., Ordóñez, C., Pope, R. J., Rumbold, S. T., Russo, M. R., Savage, N. H., Sellar, A., Stringer, M., Turnock, S. T., Wild, O., Zeng, G., and Archibald, A.: Description and evaluation of the UKCA stratosphere-troposphere chemistry scheme (StratTrop vn 1.0) implemented in UKESM1, Geosci. Model Dev, 13, 1223–1266, https://doi.org/10.5194/gmd-13-1223-2020, 2020.

Barkhordarian, A., Bowman, K. W., Cressie, N., al, Jacobson, T. W. P., Seager, R., Clarke, H., Ferreira, V., Buras, A., Zscheischler, J., Mahecha, M., and Rammig, A.: Evaluating the 2023–2024 record dry-hot conditions in the Amazon in the context of historical compound extremes, Environmental Research Letters, 20, 084 055, https://doi.org/10.1088/1748-9326/ADE550, 2025.

Belém, L. B., Albuquerque, R., Peres, L. F., Santos, F. L., Rodrigues, J. A., Menezes, L. S., Silva, P. S., Trigo, R. M., DaCamara, C. C., Russo, A., Geirinhas, J., Junior, G. A., Roque, F. O., Nunes, A. M., and Libonati, R.: Dry–Hot Compound Events Driving the 2024 Pantanal Wildfires, International Journal of Climatology, 46, e70 312, https://doi.org/10.1002/JOC.70312, 2026.

Blake, N. J., Blake, D. R., Sive, B. C., Chen, T. Y., Rowland, F. S., Collins, J. E., Sachse, G. W., and Anderson, B. E.: Biomass burning emissions and vertical distribution of atmospheric methyl halides and other reduced carbon gases in the South Atlantic region, Journal of Geophysical Research: Atmospheres, 101, 24 151–24 164, https://doi.org/10.1029/96JD00561, 1996.

Bourgoin, C., Beuchle, R., Branco, A., Carreiras, J., Ceccherini, G., Oom, D., San-Miguel-Ayanz, J., and Sedano, F.: Extensive fire-driven degradation in 2024 marks worst Amazon forest disturbance in over 2 decades, Biogeosciences, 22, 5247–5256, https://doi.org/10.5194/BG-22-5247-2025, 2025.

CAMS: Copernicus Atmosphere Monitoring Service (2022): CAMS global biomass burning emissions based on fire radiative power (GFAS), https://doi.org/10.24381/a05253c7, 2022.

https://doi.org/10.5194/egusphere-2026-6903
Preprint. Discussion started: 12 November 2026
© Author(s) 2026. CC BY 4.0 License.

Chaliyakunnel, S., Millet, D. B., Wells, K. C., Cady-Pereira, K. E., and Shephard, M. W.: A Large Underestimate of Formic Acid from Tropical Fires: Constraints from Space-Borne Measurements, Environmental Science and Technology, 50, 5631–5640, https://doi.org/10.1021/ACS.EST.5B06385, 2016.

Chen, X., Millet, D. B., Neuman, J. A., Veres, P. R., Ray, E. A., Commane, R., Daube, B. C., McKain, K., Schwarz, J. P., Katich, J. M., Froyd, K. D., Schill, G. P., Kim, M. J., Crounse, J. D., Allen, H. M., Apel, E. C., Hornbrook, R. S., Blake, D. R., Nault, B. A., Campuzano-Jost, P., Jimenez, J. L., and Dibb, J. E.: HCOOH in the Remote Atmosphere: Constraints from Atmospheric Tomography (ATom) Airborne Observations, ACS Earth and Space Chemistry, 5, 1436–1454, https://doi.org/10.1021/acsearthspacechem.1c00049, 2021.

Cope, J. D., Abellar, K. A., Bates, K. H., Fu, X., and Nguyen, T. B.: Aqueous Photochemistry of 2-Methyltetrol and Erythritol as Sources of Formic Acid and Acetic Acid in the Atmosphere, ACS Earth and Space Chemistry, 5, 1265–1277, https://doi.org/10.1021/acsearthspacechem.1c00107, 2021.

Daimari, S. R., Changmai, R. R., and Sarma, M.: Atmospheric oxidation of hydroxymethyl methyl α-lactone (HMML), initiated by OH radicals and Cl atoms, Environmental Science: Processes & Impacts, 28, 173–185, https://doi.org/10.1039/D5EM00635J, 2026.

Darbyshire, E., Morgan, W. T., Allan, J. D., Liu, D., Flynn, M. J., Dorsey, J. R., O'Shea, S. J., Lowe, D., Szpek, K., Marenco, F., Johnson, B. T., Bauguitte, S., Haywood, J. M., Brito, J. F., Artaxo, P., Longo, K. M., and Coe, H.: The vertical distribution of biomass burning pollution over tropical South America from aircraft in situ measurements during SAMBBA, Atmospheric Chemistry and Physics, 19, 5771–5790, https://doi.org/10.5194/acp-19-5771-2019, 2019.

de Laat, A. T., Andela, N., Forkel, M., Huijnen, V., Kinalczyk, D., and van Wees, D.: Sentinel-5p Reveals Unexplained Large Wildfire Carbon Emissions in the Amazon in 2024, Geophysical Research Letters, 53, e2025GL115 123, https://doi.org/10.1029/2025GL115123, 2026.

Dudhia, A.: The Reference Forward Model (RFM), Journal of Quantitative Spectroscopy and Radiative Transfer, 186, 243–253, https://doi.org/10.1016/J.JQSRT.2016.06.018, 2017.

Duncan, B. N., Strahan, S. E., Yoshida, Y., Steenrod, S. D., and Livesey, N.: Model study of the cross-tropopause transport of biomass burning pollution, Atmos. Chem. Phys, 7, 3713–3736, www.atmos-chem-phys.net/7/3713/2007/, 2007.

Esentürk, E., Abraham, N. L., Archer-Nicholls, S., Mitsakou, C., Griffiths, P., Archibald, A., and Pyle, J.: Quasi-Newton methods for atmospheric chemistry simulations: Implementation in UKCA UM vn10.8, Geoscientific Model Development, 11, 3089–3108, https://doi.org/10.5194/gmd-11-3089-2018, 2018.

Forgioni, F. P., Bresciani, C., Reis, A., Müller, G. V., Herdies, D. L., Júnior, J. B. C., and dos Santos Silva, F. D.: Aerosol Transport from Amazon Biomass Burning to Southern Brazil: A Case Study of an Extreme Event During September 2024, Atmosphere, 16, 1138, https://doi.org/10.3390/atmos16101138, 2025.

Franco, B., Blumenstock, T., Cho, C., Clarisse, L., Clerbaux, C., Coheur, P. F., Mazière, M. D., Smedt, I. D., Dorn, H. P., Emmerichs, T., Fuchs, H., Gkatzelis, G., Griffith, D. W., Gromov, S., Hannigan, J. W., Hase, F., Hohaus, T., Jones, N., Kerkweg, A., Kiendler-Scharr, A., Lutsch, E., Mahieu, E., Novelli, A., Ortega, I., Paton-Walsh, C., Pommier, M., Pozzer, A., Reimer, D., Rosanka, S., Sander, R., Schneider, M., Strong, K., Tillmann, R., Roozendael, M. V., Vereecken, L., Vigouroux, C., Wahner, A., and Taraborrelli, D.: Ubiquitous atmospheric production of organic acids mediated by cloud droplets, Nature 2021 593:7858, 593, 233–237, https://doi.org/10.1038/s41586-021-03462-x, 2021.

Friedman, B., Link, M. F., Fulgham, S. R., Brophy, P., Galang, A., Brune, W. H., Jathar, S. H., and Farmer, D. K.: Primary and Secondary Sources of Gas-Phase Organic Acids from Diesel Exhaust, Environmental Science and Technology, 51, 10 872–10 880, https://doi.org/10.1021/ACS.EST.7B01169, 2017.

https://doi.org/10.5194/egusphere-2026-6903
Preprint. Discussion started: 12 November 2026
© Author(s) 2026. CC BY 4.0 License.

Giglio, L.: MODIS Collection 5 Active Fire Product User's Guide: Version 2.5, Science Systems and Applications, Inc, https://gsweb10.umd.edu/files/MODIS_Fire_Users_Guide_2.5.pdf, 2013.

Glatthor, N., Stiller, G. P., von Clarmann, T., Funke, B., Kellmann, S., and Linden, A.: Upper-tropospheric pollutants observed by MIPAS: geographic and seasonal variations, Atmospheric Chemistry and Physics, 25, 1175–1208, https://doi.org/10.5194/acp-25-1175-2025, 2025.

Gonzalez-Alonso, L., Martin, M. V., and Kahn, R. A.: Biomass-burning smoke heights over the Amazon observed from space, Atmospheric Chemistry and Physics, 19, 1685–1702, https://doi.org/10.5194/ACP-19-1685-2019, 2019.

Goudar, M., Anema, J. C., Kumar, R., Borsdorff, T., and Landgraf, J.: Plume detection and emission estimate for biomass burning plumes from TROPOMI carbon monoxide observations using APE v1.1, Geoscientific Model Development, 16, 4835–4852, https://doi.org/10.5194/GMD-16-4835-2023, 2023.

Guyon, P., Frank, G. P., Welling, M., Chand, D., Artaxo, P., Rizzo, L., Nishioka, G., Kolle, O., Fritsch, H., Dias, M. A. S., Gatti, L. V., Cordova, A. M., and Andreae, M. O.: Airborne measurements of trace gas and aerosol particle emissions from biomass burning in Amazonia, Atmospheric Chemistry and Physics, 5, 2989–3002, https://doi.org/10.5194/ACP-5-2989-2005, 2005.

Hodgson, A. K., Morgan, W. T., O'Shea, S., Bauguitte, S., Allan, J. D., Darbyshire, E., Flynn, M. J., Liu, D., Lee, J., Johnson, B., Haywood, J. M., Longo, K. M., Artaxo, P. E., and Coe, H.: Near-field emission profiling of tropical forest and Cerrado fires in Brazil during SAMBBA 2012, Atmospheric Chemistry and Physics, 18, 5619–5638, https://doi.org/10.5194/ACP-18-5619-2018, 2018.

Illingworth, S. M., Remedios, J. J., Boesch, H., Moore, D. P., Sembhi, H., Dudhia, A., and Walker, J. C.: ULIRS, an optimal estimation retrieval scheme for carbon monoxide using IASI spectral radiances: Sensitivity analysis, error budget and simulations, Atmospheric Measurement Techniques, 4, 269–288, https://doi.org/10.5194/AMT-4-269-2011, 2011.

Jang, M., Czoschke, N. M., Lee, S., and Kamens, R. M.: Heterogeneous Atmospheric Aerosol Production by Acid-Catalyzed Particle-Phase Reactions, Science, 298, 814–817, https://doi.org/10.1126/science.1075798, 2002.

Jenkin, M. E., Young, J. C., and Rickard, A. R.: The MCM v3.3.1 degradation scheme for isoprene, Atmospheric Chemistry and Physics, 15, 11 433–11 459, https://doi.org/10.5194/ACP-15-11433-2015, 2015.

Jiang, Y., Xia, M., Wang, Z., Zheng, P., Chen, Y., and Wang, T.: Photochemical ageing of aerosols contributes significantly to the production of atmospheric formic acid, Atmos. Chem. Phys, 23, 14 813–14 828, https://doi.org/10.5194/acp-23-14813-2023, 2023.

Johansson, S., Wetzel, G., Friedl-Vallon, F., Glatthor, N., Höpfner, M., Kleinert, A., Neubert, T., Sinnhuber, B. M., and Ungermann, J.: Biomass burning pollution in the South Atlantic upper troposphere: GLORIA trace gas observations and evaluation of the CAMS model, Atmospheric Chemistry and Physics, 22, 3675–3691, https://doi.org/10.5194/ACP-22-3675-2022, 2022.

Jury, M. R., Pabón, A. R. G., Jury, M. R., and Pabón, A. R. G.: Dispersion of Smoke Plumes over South America, Earth Interactions, 25, 1–14, https://doi.org/10.1175/EI-D-20-0004.1, 2021.

Kelly, J. M., Doherty, R. M., O'Connor, F. M., Mann, G. W., Coe, H., and Liu, D.: The roles of volatile organic compound deposition and oxidation mechanisms in determining secondary organic aerosol production: a global perspective using the UKCA chemistry–climate model (vn8.4), Geoscientific Model Development, 12, 2539–2569, https://doi.org/10.5194/gmd-12-2539-2019, 2019.

Kesselmeier, J., Bode, K., Gerlach, C., and Jork, E. M.: Exchange of atmospheric formic and acetic acids with trees and crop plants under controlled chamber and purified air conditions, Atmospheric Environment, 32, 1765–1775, https://doi.org/10.1016/S1352-2310(97)00465-2, 1998.

Kluge, F., Hüneke, T., Knecht, M., Lichtenstern, M., Rotermund, M., Schlager, H., Schreiner, B., and Pfeilsticker, K.: Profiling of formaldehyde, glyoxal, methylglyoxal, and CO over the Amazon: normalized excess mixing ratios and related emission factors in biomass burning plumes, Atmospheric Chemistry and Physics, 20, 12 363–12 389, https://doi.org/10.5194/acp-20-12363-2020, 2020.

https://doi.org/10.5194/egusphere-2026-6903
Preprint. Discussion started: 12 November 2026
© Author(s) 2026. CC BY 4.0 License.

Link, M. F., Nguyen, T. B., Bates, K., Müller, J. F., and Farmer, D. K.: Can Isoprene Oxidation Explain High Concentrations of Atmospheric Formic and Acetic Acid over Forests?, ACS Earth and Space Chemistry, 4, 730–740, https://doi.org/10.1021/ACSEARTHSPACECHEM.0C00010, 2020.

Luo, P.-L., Chen, I.-Y., Khan, M. A. H., and Shallcross, D. E.: Direct gas-phase formation of formic acid through reaction of Criegee intermediates with formaldehyde, Communications Chemistry, 6, 130, https://doi.org/10.1038/s42004-023-00933-2, 2023.

Lv, S., Wang, F., Wu, C., Chen, Y., Liu, S., Zhang, S., Li, D., Du, W., Zhang, F., Wang, H., Huang, C., Fu, Q., Duan, Y., and Wang, G.: Gas-to-Aerosol Phase Partitioning of Atmospheric Water-Soluble Organic Compounds at a Rural Site in China: An Enhancing Effect of NH3 on SOA Formation, Environmental Science & Technology, 56, 3915–3924, https://doi.org/10.1021/ACS.EST.1C06855, 2022.

Marenco, F., Johnson, B., Langridge, J. M., Mulcahy, J., Benedetti, A., Remy, S., Jones, L., Szpek, K., Haywood, J., Longo, K., and Artaxo, P.: On the vertical distribution of smoke in the Amazonian atmosphere during the dry season, Atmospheric Chemistry and Physics, 16, 2155–2174, https://doi.org/10.5194/acp-16-2155-2016, 2016.

Methven, J., Arnold, S. R., O'Connor, F. M., Barjat, H., Dewey, K., Kent, J., and Brough, N.: Estimating photochemically produced ozone throughout a domain using flight data and a Lagrangian model, Journal of Geophysical Research: Atmospheres, 108, 4271, https://doi.org/10.1029/2002JD002955, 2003.

Millet, D. B., Baasandorj, M., Farmer, D. K., Thornton, J. A., Baumann, K., Brophy, P., Chaliyakunnel, S., Gouw, J. A. D., Graus, M., Hu, L., Koss, A., Lee, B. H., Lopez-Hilfiker, F. D., Neuman, J. A., Paulot, F., Peischl, J., Pollack, I. B., Ryerson, T. B., Warneke, C., Williams, B. J., and Xu, J.: A large and ubiquitous source of atmospheric formic acid, Atmospheric Chemistry and Physics, 15, 6283–6304, https://doi.org/10.5194/ACP-15-6283-2015, 2015.

Mokhov, I. I. and Akperov, M. G.: Tropospheric lapse rate and its relation to surface temperature from reanalysis data, Izvestiya, Atmospheric and Oceanic Physics 2006 42:4, 42, 430–438, https://doi.org/10.1134/S0001433806040037, 2006.

Moore, D. and Remedios, J.: EOCIS: Total Column CO Product, V1.0, https://doi.org/https://dx.doi.org/10.5285/4b31d47716604b9f84714fab39ce973c, 2025.

Morgan, W. T., Allan, J. D., Bower, K. N., Esselborn, M., Harris, B., Henzing, J. S., Highwood, E. J., Kiendler-Scharr, A., McMeeking, G. R., Mensah, A. A., Northway, M. J., Osborne, S., Williams, P. I., Krejci, R., and Coe, H.: Enhancement of the aerosol direct radiative effect by semi-volatile aerosol components: airborne measurements in North-Western Europe, Atmospheric Chemistry and Physics, 10, 8151–8171, https://doi.org/10.5194/acp-10-8151-2010, 2010.

Myhre, G., Stordal, F., Johnsrud, M., Kaufman, Y. J., Rosenfeld, D., Storelvmo, T., Kristjansson, J. E., Berntsen, T. K., Myhre, A., and Isaksen, I. S.: Aerosol-cloud interaction inferred from MODIS satellite data and global aerosol models, Atmospheric Chemistry and Physics, 7, 3081–3101, https://doi.org/10.5194/ACP-7-3081-2007, 2007.

NASA: MOD04_L2 - MODIS/Terra Aerosol 5Min L2 Swath 10km, https://catalogue.ceda.ac.uk/uuid/f5e2886edf254a42804b9a77af6d5c9c/, 2021.

Nguyen, T. B., Bates, K. H., Crounse, J. D., Schwantes, R. H., Zhang, X., Kjaergaard, H. G., Surratt, J. D., Lin, P., Laskin, A., Seinfeld, J. H., and Wennberg, P. O.: Mechanism of the hydroxyl radical oxidation of methacryloyl peroxynitrate (MPAN) and its pathway toward secondary organic aerosol formation in the atmosphere, Physical Chemistry Chemical Physics, 17, 17 914–17 926, https://doi.org/10.1039/C5CP02001H, 2015.

Nguyen, T. L., Peeters, J., Müller, J. F., Perera, A., Bross, D. H., Ruscic, B., and Stanton, J. F.: Methanediol from cloud-processed formaldehyde is only a minor source of atmospheric formic acid, Proceedings of the National Academy of Sciences of the United States of America, 120, e2304650 120, https://doi.org/10.1073/pnas.2304650120, 2023.

https://doi.org/10.5194/egusphere-2026-6903
Preprint. Discussion started: 12 November 2026
© Author(s) 2026. CC BY 4.0 License.



O'Connor, F. M., Johnson, C. E., Morgenstern, O., Abraham, N. L., Braesicke, P., Dalvi, M., Folberth, G. A., Sanderson, M. G., Telford, P. J., Voulgarakis, A., Young, P. J., Zeng, G., Collins, W. J., and Pyle, J. A.: Evaluation of the new UKCA climate-composition model-Part 2: The troposphere, Geoscientific Model Development, 7, 41–91, https://doi.org/10.5194/GMD-7-41-2014, 2014.

Paulot, F., Wunch, D., Crounse, J. D., Toon, G. C., Millet, D. B., Decarlo, P. F., Vigouroux, C., Deutscher, N. M., Abad, G. G., Notholt, J., Warneke, T., Hannigan, J. W., Warneke, C., Gouw, J. A. D., Dunlea, E. J., Mazière, M. D., Griffith, D. W., Bernath, P., Jimenez, J. L., and Wennberg, P. O.: Importance of secondary sources in the atmospheric budgets of formic and acetic acids, Atmospheric Chemistry and Physics, 11, 1989–2013, https://doi.org/10.5194/ACP-11-1989-2011, 2011.

Permar, W., Wielgasz, C., Jin, L., Chen, X., Coggon, M. M., Garofalo, L. A., Gkatzelis, G. I., Ketcherside, D., Millet, D. B., Palm, B. B., Peng, Q., Robinson, M. A., Thornton, J. A., Veres, P., Warneke, C., Yokelson, R. J., Fischer, E. V., and Hu, L.: Assessing formic and acetic acid emissions and chemistry in western U.S. wildfire smoke: implications for atmospheric modeling, Environmental Science: Atmospheres, 3, 1620–1641, https://doi.org/10.1039/D3EA00098B, 2023.

Pommier, M., Clerbaux, C., and Coheur, P.-F.: Determination of enhancement ratios of HCOOH relative to CO in biomass burning plumes by the Infrared Atmospheric Sounding Interferometer (IASI), Atmos. Chem. Phys, 17, 11 089–11 105, https://doi.org/10.5194/acp-17-11089-2017, 2017.

Ramos, A. M., Blamey, R. C., Algarra, I., Nieto, R., Gimeno, L., Tomé, R., Reason, C. J., and Trigo, R. M.: From Amazonia to southern Africa: atmospheric moisture transport through low-level jets and atmospheric rivers, Annals of the New York Academy of Sciences, 1436, 217–230, https://doi.org/10.1111/NYAS.13960, 2019.

Ranaivombola, M., Bègue, N., Peres, L. V., Fazel-Rastgar, F., Sivakumar, V., Krysztofiak, G., Berthet, G., Jegou, F., Piketh, S., and Bencherif, H.: Characterization of aerosol optical depth (AOD) anomalies in September and October 2022 over Skukuza in South Africa, Atmospheric Chemistry and Physics, 25, 3519–3540, https://doi.org/10.5194/ACP-25-3519-2025, 2025.

R'honi, Y., Clarisse, L., Clerbaux, C., Hurtmans, D., Duflot, V., Turquety, S., Ngadi, Y., and Coheur, P.-F.: Sciences ess Atmospheric Chemistry and Physics Climate of the Past Geoscientific Instrumentation Methods and Data Systems Exceptional emissions of NH 3 and HCOOH in the 2010 Russian wildfires, Atmos. Chem. Phys, 13, 4171–4181, https://doi.org/10.5194/acp-13-4171-2013, 2013.

Rémy, S., Veira, A., Paugam, R., Sofiev, M., Kaiser, J. W., Marenco, F., Burton, S. P., Benedetti, A., Engelen, R. J., Ferrare, R., and Hair, J. W.: Two global data sets of daily fire emission injection heights since 2003, Atmospheric Chemistry and Physics, 17, 2921–2942, https://doi.org/10.5194/acp-17-2921-2017, 2017.

Sanhueza, E. and Andreae, M. O.: Emission of formic and acetic acids from tropical Savanna soils, Geophysical Research Letters, 18, 1707–1710, https://doi.org/10.1029/91GL01565;PAGEGROUP:STRING:PUBLICATION, 1991.

Santos, F., Longo, K., Guenther, A., Kim, S., Gu, D., Oram, D., Forster, G., Lee, J., Hopkins, J., Brito, J., and Freitas, S.: Biomass burning emission disturbances of isoprene oxidation in a tropical forest, Atmos. Chem. Phys, 18, 12 715–12 734, https://doi.org/10.5194/acp-18-12715-2018, 2018.

Signori, R. T., Mamani, L., Cevalho, W., de Souza, I. P., Kayano, M. T., de Oliveira, M. B. L., Céron, W. L., Andreoli, R. V., and de Souza, R. A. F.: How climate variability modes influenced the fires in South America during the extreme droughts of 2023–2024, Science of The Total Environment, 1028, 181 705, https://doi.org/10.1016/J.SCITOTENV.2026.181705, 2026.

Silva, M., Eisa, M., Ragauskaitė, D., and Baltrusaitis, J.: Water Sorption on Formic Acid-Modified Hydroxyapatite as a Function of Relative Humidity: Simulated Environmental Aging Effects on Hygroscopicity and Nutrient Release, ACS Earth and Space Chemistry, 6, 3043–3053, https://doi.org/10.1021/acsearthspacechem.2c00273, 2022.

https://doi.org/10.5194/egusphere-2026-6903
Preprint. Discussion started: 12 November 2026
© Author(s) 2026. CC BY 4.0 License.



Spracklen, D. V., Pringle, K. J., Carslaw, K. S., Chipperfield, M. P., and Mann, G. W.: A global off-line model of size-resolved aerosol microphysics: I. Model development and prediction of aerosol properties, Atmospheric Chemistry and Physics, 5, 2227–2252, https://doi.org/10.5194/ACP-5-2227-2005, 2005.

Stavrakou, T., Müller, J.-F., Peeters, J., Razavi, A., Clarisse, L., Clerbaux, C., Coheur, P.-F., Hurtmans, D., Mazière, M. D., Vigouroux, C., Deutscher, N. M., Griffith, D. W. T., Jones, N., and Paton-Walsh, C.: Satellite evidence for a large source of formic acid from boreal and tropical forests, Nature Geoscience, 5, 26–30, https://doi.org/10.1038/ngeo1354, 2012.

Surratt, J. D., Lewandowski, M., Offenberg, J. H., Jaoui, M., Kleindienst, T. E., Edney, E. O., and Seinfeld, J. H.: Effect of Acidity on Secondary Organic Aerosol Formation from Isoprene, Environmental Science & Technology, 41, 5363–5369, https://doi.org/10.1021/es0704176, 2007.

Tan, F., Zhang, H., Xia, K., Jing, B., Li, X., Tong, S., and Ge, M.: Hygroscopic behavior and aerosol chemistry of atmospheric particles containing organic acids and inorganic salts, npj Climate and Atmospheric Science, 7, 203, https://doi.org/10.1038/s41612-024-00752-9, 2024.

Tereszchuk, K. A., Abad, G. G., Clerbaux, C., Hurtmans, D., Coheur, P.-F., and Bernath, P. F.: ACE-FTS measurements of trace species in the characterization of biomass burning plumes, Atmos. Chem. Phys, 11, 12 169–12 179, https://doi.org/10.5194/acp-11-12169-2011, 2011.

Tilgner, A., Schaefer, T., Alexander, B., Barth, M., Collett, J. L., Fahey, K. M., Nenes, A., Pye, H. O., Herrmann, H., and McNeill, V. F.: Acidity and the multiphase chemistry of atmospheric aqueous particles and clouds, Atmospheric Chemistry and Physics, 21, 13 483–13 536, https://doi.org/10.5194/ACP-21-13483-2021, 2021.

van der Werf, G. R., Randerson, J. T., van Wees, D., Chen, Y., Giglio, L., Hall, J., Roland, V., Mu, M., Shahid, S. B., Barsanti, K. C., Yokelson, R., and Morton, D. C.: Landscape fire emissions from the 5th version of the Global Fire Emissions Database (GFED5), Scientific Data 2025 12:1, 12, 1870–, https://doi.org/10.1038/s41597-025-06127-w, 2025.

Velásquez-García, M. P., Pope, R. J., Turnock, S. T., Deva, C., Moore, D. P., Mataveli, G., Arnold, S. R., Doherty, R. M., and Chipperfield, M. P.: Understanding drivers and biases of simulated CO emissions from the INFERNO fire model over South America, Biogeosciences, 23, 1341–1364, https://doi.org/10.5194/BG-23-1341-2026, 2026.

Viatte, C., Strong, K., Hannigan, J., Nussbaumer, E., Emmons, L. K., Conway, S., Paton-Walsh, C., Hartley, J., Benmergui, J., and Lin, J.: Identifying fire plumes in the Arctic with tropospheric FTIR measurements and transport models, Atmospheric Chemistry and Physics, 15, 2227–2246, https://doi.org/10.5194/acp-15-2227-2015, 2015.

Vigouroux, C., Aquino, C. A. B., Mazière, M. D., Gatti, L., Kumps, N., and Langerock, B.: FTIR formic acid (HCOOH) groundbased remote sensing at Porto Velho from instrument BIRA.IASB004, https://doi.org/https://doi.org/10.18758/lguyweqe, 2021.

Wizenberg, T., Strong, K., Jones, D. B., Lutsch, E., Mahieu, E., Franco, B., and Clarisse, L.: Exceptional Wildfire Enhancements of PAN, C2H4, CH3OH, and HCOOH Over the Canadian High Arctic During August 2017, Journal of Geophysical Research: Atmospheres, 128, e2022JD038 052, https://doi.org/10.1029/2022JD038052, 2023.

Yamanouchi, S., Strong, K., Lutsch, E., and Jones, D. B. A.: Detection of HCOOH, CH 3 OH, CO, HCN, and C 2 H 6 in Wildfire Plumes Transported Over Toronto Using Ground-Based FTIR Measurements From 2002-2018, Journal of Geophysical Research: Atmospheres, 125, e2019JD031 924, https://doi.org/10.1029/2019JD031924, 2020.

Yokelson, R. J., Crounse, J. D., DeCarlo, P. F., Karl, T., Urbanski, S., Atlas, E., Campos, T., Shinozuka, Y., Kapustin, V., Clarke, A. D., Weinheimer, A., Knapp, D. J., Montzka, D. D., Holloway, J., Weibring, P., Flocke, F., Zheng, W., Toohey, D., Wennberg, P. O., Wiedinmyer, C., Mauldin, L., Fried, A., Richter, D., Walega, J., Jimenez, J. L., Adachi, K., Buseck, P. R., Hall, S. R., and Shetter, R.: Emissions from biomass burning in the Yucatan, Atmospheric Chemistry and Physics, 9, 5785–5812, https://doi.org/10.5194/ACP-9-5785-2009, 2009.

https://doi.org/10.5194/egusphere-2026-6903
Preprint. Discussion started: 12 November 2026
© Author(s) 2026. CC BY 4.0 License.



Yu, S.: Role of organic acids (formic, acetic, pyruvic and oxalic) in the formation of cloud condensation nuclei (CCN): a review, Atmospheric Research, 53, 185–217, https://doi.org/10.1016/S0169-8095(00)00037-5, 2000.

Zhang, W., Xu, L., Thadiyampurath, S., Liu, X., Leong, T., Pagonis, D., Campuzano-Jost, P., Jimenez, J. L., Robinson, M. A., Veres, P., DiGangi, J., Halliday, H., Nowak, J., Diskin, G. S., and Zhang, H.: Rapid Levoglucosan Oxidation as a Key Process in Biomass Burning Aerosol Aging, Environmental Science & Technology, 60, 983–995, https://doi.org/10.1021/ACS.EST.5C14970, 2025.